

USE OF THE MOIRE METHOD IN THE ANALYSIS OF RECTANGULAR
BALCONY GIRDER FRAMES

by

HASAN KAMIL

B.Sc. Engg.(Civil), Aligarh Muslim University(INDIA), 1964

A MASTER'S THESIS

submitted in partial fulfillment of the
requirements for the degree

MASTER OF SCIENCE

Department of Civil Engineering

KANSAS STATE UNIVERSITY

Manhattan, Kansas

1967

Approved by:

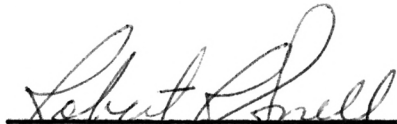

Major Professor

TABLE OF CONTENTS

	Page
LIST OF FIGURES.iii
LIST OF TABLES	v
ACKNOWLEDGEMENTS	vi
INTRODUCTION	1
REVIEW OF LITERATURE	3
REVIEW OF THE MOIRE METHOD	6
EQUIPMENT AND TEST PROCEDURE	12
TESTING SEQUENCE AND DETERMINATION OF TIME DEPENDENT MODULUS, E_t	19
GENERAL CHARACTERISTICS OF FRINGE PATTERNS	23
PRESENTATION AND EVALUATION OF EXPERIMENTAL RESULTS.	24
DEVELOPMENT OF THEORETICAL RESULTS TO BE COMPARED WITH EXPERIMENTAL RESULTS	48
COMPARISON AND DISCUSSION OF RESULTS	70
SUMMARY AND CONCLUSIONS.	84
RECOMMENDATIONS FOR FURTHER RESEARCH	86
LIST OF SYMBOLS.	87
BIBLIOGRAPHY	88
APPENDIX	90

LIST OF FIGURES

	Page
Figure 1. General setup and the principle of the Moire method.	8
Figure 2. Error made by using the formula $PQ = 2a\phi$	9
Figure 3. Sample Fringe pattern	11
Figure 4. Moire Fringe apparatus.	13
Figure 5. Details of loading arrangement and model supports.	15
Figure 6. Models with their load positions.	17
Figure 7. Variation of E_t with time for plexiglas	20
Figure 8. Model No. 1	26
Figure 9. Fringe Photographs with grid lines horizontal	29
Figure 10. Fringe order versus distance curve for leg AC with load at sta. 5	30
Figure 11. Bending Moment diagram for leg AC with load at sta. 5.	32
Figure 12. Shear Force diagram for leg AC with load at sta. 5.	32
Figure 13. Fringe order versus distance curve for leg BD with load at sta. 5	33
Figure 14. Bending Moment diagram for leg BD with load at sta. 5.	35
Figure 15. Shear Force diagram for leg BD with load at sta. 5.	35
Figure 16. Fringe photographs with grid lines vertical	36
Figure 17. Fringe order versus distance curve for beam CD with load at sta. 5	37
Figure 18. Bending Moment diagram for beam CD with load at sta. 5	38

Figure 19. Shear Force diagram for beam CD with load at sta. 5.	38
Figure 20. Fringe order versus distance curve for leg AC with load at sta. 5	41
Figure 21. Torsional Moment diagram for leg AC or BD, with load at sta. 5	42
Figure 22. Torsional Moment diagram for beam CD with load at sta. 5	44
Figure 23-24. Theoretical Bending Moment and Shear Force diagrams for the leg AC with load at sta. 5	65
Figure 25-26. Theoretical Bending Moment and Shear Force diagrams for leg BD with load at sta. 5	66
Figure 27-28. Theoretical Bending Moment and Shear Force diagrams for beam CD with load at sta. 5.	67
Figure 29. Theoretical Torsional Moment diagram for leg AC or BD with load at sta. 5	68
Figure 30. Theoretical Torsional Moment diagram for beam CD with load at sta. 5.	69
Figure 31-33. Influence Line diagrams for model No. 1.	76-78
Figure 34-36. Influence Line diagrams for model No. 2.	79-81
Figure 37-39. Influence Line diagrams for model No. 3.	82-83
Figure 40. Figure used for the derivation of the formula $PQ = 2a\phi(1 + c^2/a^2)$	90

LIST OF TABLES

	Page
Table No. 1. Experimental Determination of E_t for 4.5 minutes time of application of load.	22
Table Nos. 2-4. Final Experimental Results	45-47
Table Nos. 5-7. Values of Bending and Torsional Moments at different sections of the model	59-60
Table Nos. 8-10. Theoretical Results.	62-64
Table Nos. 11-13. Comparison of Experimental and Theoretical Results.	73-75

ACKNOWLEDGEMENTS

I wish to express my most sincere appreciation and thanks for the direction and guidance given by Dr. Robert R. Snell, Associate Professor of Civil Engineering at Kansas State University. Without his efforts and encouragement, this research would not have been possible.

For his valuable suggestions in the organization and review of this thesis, I would like to extend my sincere thanks to Dr. Jack B. Blackburn, Head of the Civil Engineering Department at Kansas State University.

INTRODUCTION

The Moire method, although recent in origin, has been found to be an effective and efficient method for the analysis of various plate or grid structures. Because it requires a simple apparatus and relatively easy computations, it is quite useful. In particular, it is helpful in the analysis of structures which otherwise would require complex mathematical calculations for their solution.

The Moire effect is an optical phenomenon produced when two somewhat similar arrays of dots or lines are superimposed, resulting in the formation of light and dark fringes. When used for the analysis of structures, the changes in slope, due to loading, of all the points on the model are determined by, first, taking a photograph of the image of a lined screen reflected by the unloaded model and then photographing on the same negative, the reflection of the lined screen from the loaded model. From the known slopes, it is then possible to determine the curvatures of the model, and the bending and torsion moments.

The purpose of this study was:

- (1) to demonstrate the use of the Moire method for the analysis of a fairly complex rectangular balcony girder frame and hence to show its usefulness for the analysis of many types of complex structures,
- (2) to study the behaviour of rectangular balcony girder frames under stationary and moving loads,
- (3) to derive a set of general equations for the theoretical analysis of rectangular balcony girder frames using a strain energy method, and to use them for the verification of the experimental results.

An overhanging balcony girder frame, whether rectangular or curved or of any other shape, can be analysed experimentally or theoretically by any of several different methods i.e. photoelastic method, deflection determination method, slope deflection method, or by any of the strain energy methods. But, as shown in this study, the Moire method, by virtue of its simplicity, can be considered as a very useful method for the analysis of these types of structures.

REVIEW OF LITERATURE

The Moire method in its present form, was developed by Lightenberg (1), at the Technological University of Delft in the Netherlands in 1954, who applied it to small slab models. His models included a rectangular plate with a circular hole, an equilateral triangular plate, a skew slab bridge model, and a floor panel with numerous holes. The experimental results he obtained from the models gave excellent agreement with the theoretical results.

In the same year, Vreendenburgh and Van Wijngarden published a paper (2) dealing with the determination of the distribution of moments in flat slabs, using the Moire method. Their results were checked with experiments carried out by the National Council of Applied Scientific Research in the Netherlands, and with the exception of a single result, very good agreement was found.

In 1956, Bradley used the Moire method to study the effect of a rectangular cutout in a square clamped plate on the distribution of moments in the plate (20). He verified the experimental results of his study by the use of an approximate theoretical analysis, making use of finite differences. He used black perspex as his model material and introduced a lever system for the application of concentrated loads and aircells for uniformly distributed loads. The grid line spacing was 0.05 inches. He tested, in all, five models, and the results he obtained experimentally were in very close agreement with the theoretical results, with a maximum difference of about $\pm 5\%$.

In 1960, Morse, Durelli, and Sciammarella presented the results of their study on the use of the Moire method in the two dimensional analysis

of strains (3).

In the same year, Durelli along with Daniel presented a paper demonstrating the use of Moire fringes in the measurement of displacements and rotations in structural models (4). A modified method was developed by the use of two grids instead of one, a "model grid" cemented to the model and a fixed grid referred to as the "master grid", with respect to which the displacements could be measured. The grids used were transparent and were assumed to be in the same plane.

In the same year, Durelli and Sciammarella started work on the interpretation of the Moire patterns as a function of displacements. A paper was published in 1961 (5). They also used two transparent grids. In 1963, Durelli, Sciammarella, and Parks presented a paper dealing with the detailed analysis of some points in the basic laws of Moire patterns (6). Properties dealing with the uniqueness and continuity of displacements were examined, so that the study provided a means to interpret the most general type of Moire patterns for strain analysis.

In the same year, Sciammarella along with Fu-Pen Chiang developed a technique to extend the Moire method to three-dimensional problems (7). The test results showed that the accuracy and the sensitivity of the method were satisfactory.

In a paper published in the same year, Bouwkamp discussed, in relation to the Moire method as used for the solution of plate bending, two graphical techniques for the determination of the direction of principal moments and stresses (8).

In June, 1964, Theocaris discussed the plane stress problems in relation to the Moire method (9). In the same year, Kubitza presented the

results of his work on stress analysis of grid works using the Moire method in the form of his Ph.D. dissertation at Washington University (10). He used a slightly modified apparatus and technique to obtain his results. He reduced the width of the screen ruling to $1/12$ " and used four fluorescent tubes around his model. He also revised the photographic procedure and used a 35 mm. camera with a high contrast copy film. All of his models were made of black plexiglas. His work yielded results which were within 3.5% agreement with the calculated results.

In a paper published in August 1965, Theocaris and Kuo presented a theory of Moire fringes produced by zonal gratings interfering with line gratings (11).

In November, 1965, Post discussed the Moire grid analyser method for strain analysis (12). Also, in the same year, Fu Pen Chiang discussed a more accurate plotting method for displacement curves by using two-grids (13). In April, 1966, Theocaris discussed the use of the Moire method for the measurement of partial slopes in flexed plates (14).

The Moire method has also been extended to thermal problems in recent years and a great deal of work is still being done in that area. In one of the most recent papers on Moire method, published in May 1966, Sciammarella and Sturgeon discussed the use of the Moire method in the determination of thermal stresses at high temperatures in stainless steel rings (15).

REVIEW OF THE MOIRE METHOD

The Moire method, as already mentioned, has a real advantage over many other experimental methods of stress analysis in its direct determination of the slope at any point on the model in any desired direction. The determination of slope is achieved by the use of a simple apparatus which essentially consists of the following parts:

- a) A grid or a ruled screen, consisting of alternate black and white lines of equal width,
- b) A camera, used to record two exposures on the same negative: first the reflection of the grid by the unloaded model; and second, the reflection of the grid by the loaded model,
- c) A model with a good reflecting surface.

These three parts are supported by a massive and very rigid metal or wooden frame.

The arrangement of these parts and the basic principle of the Moire method are shown in Fig. 1.

The first exposure is made of the unloaded model. The point P on the screen is reflected by the point R on the model to appear as point I on the film in the camera. The next exposure is, then, taken of the loaded model so that the point R now shifts to point R'. The model rotates through an angle, say ϕ , and the point I on the film now becomes the image of the point Q instead of P on the screen. The relationship between the rotation of the model and the distance PQ on the screen, for a flat screen, can be written as below:

$$PQ = 2\phi a \left(1 + \frac{c^2}{a^2}\right)$$

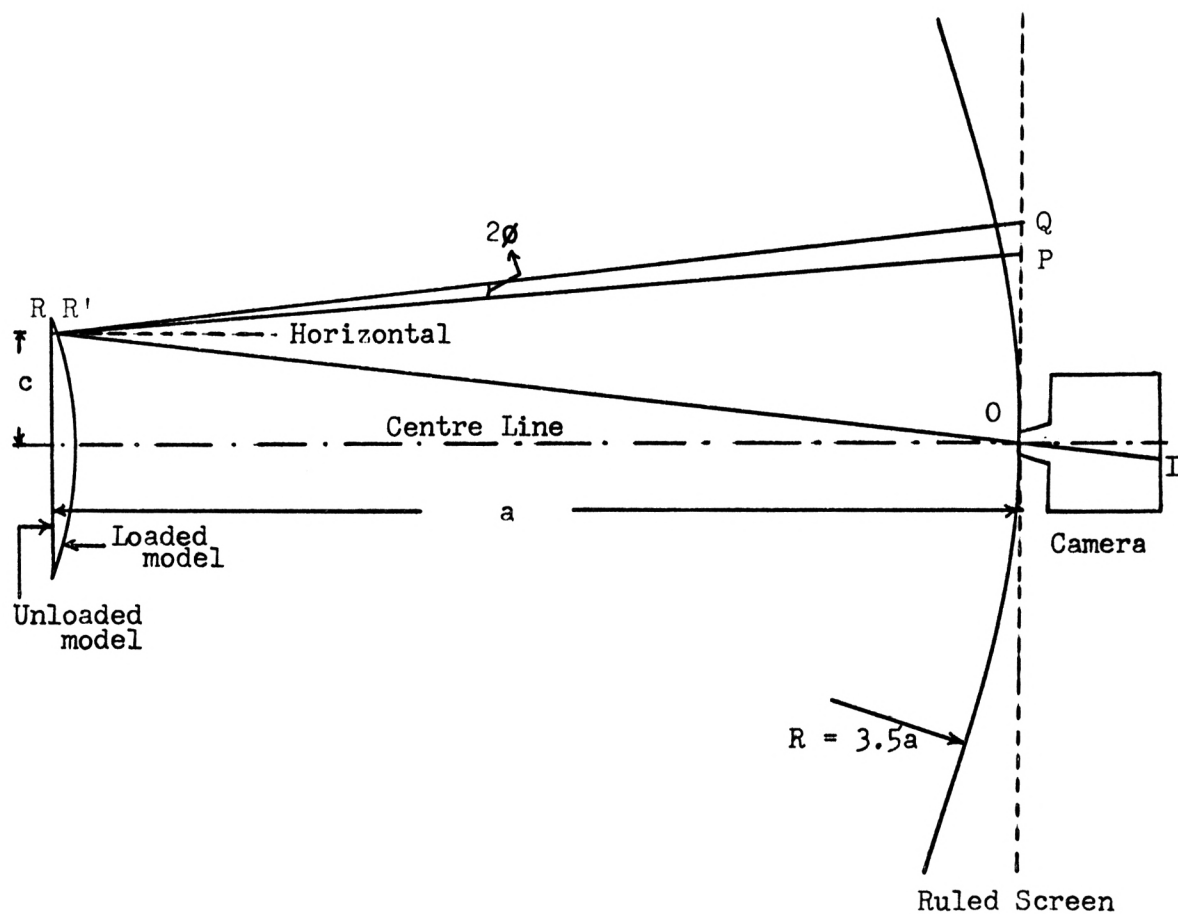
The derivation of this formula is given in the appendix.

If the distance between the point R on the model and its axis is not too great, the term $\frac{c^2}{a^2}$ will be very small and can be neglected for a flat screen. With $a = 25"$, say, and with an 8" model (max. $c = 4"$), an error of about $2\frac{1}{2}\%$ would result if ϕ were taken to be equal to $\frac{PQ}{2a}$. However, this error can be theoretically eliminated and practically reduced to a negligible amount by the use of a curved screen, as suggested by Lightenberg (1). With a radius of cylindrical screen equal to 3.5 times a , we will have

$$\phi = \frac{PQ}{2a}, \text{ for all practical purposes.}$$

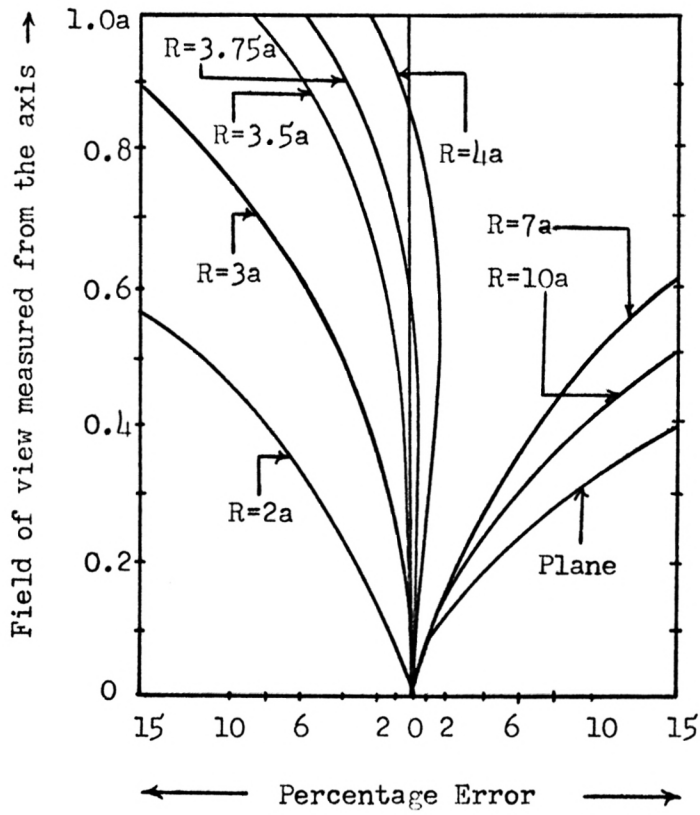
Fig. 2 shows the deviation of the true values of ϕ from $PQ/2a$ for different values of the radius of the screen, as computed by Lightenberg (1).

The distance PQ is known, as the ruled screen or the grid has the same definite spacing for two black or white lines on it. By superimposing the exposures of the loaded and the unloaded models on the same negative, the Moire fringes will appear in a definite pattern. They will consist of alternate light and dark stripes or bands. The light bands are generated by the compensation of the two exposures of the P and Q portions into full exposure of the area. These light bands are known as "Half fringes", because they locate the points undergoing a rotation of $\frac{2n-1}{2}(\frac{d}{2a})$, where $n = 1, 2, 3, \dots$; and so, are of the order $\frac{1}{2}, 1\frac{1}{2}, 2\frac{1}{2}, 3\frac{1}{2}, 4\frac{1}{2}, \dots$, respectively. Similarly, the dark bands or stripes are produced when the P region coincides with the Q region, so that white lines coincide with white lines and black lines coincide with black lines. These bands are



General setup and the principle of the Moire method

Fig. 1



Error made by using the formula $PQ = 2a\phi(1)$

Fig. 2

known as the "Integer fringes", as they locate the points undergoing a rotation of zero, $1\frac{d}{2a}$, $2\frac{d}{2a}$, $3\frac{d}{2a}$,.....; and so, are of the order 0, 1, 2, 3,....., respectively.

Every fringe of the set represents the points on the surface of the model which have a particular value of the slope in a direction perpendicular to the screen rulings. One can, therefore, have a general idea about the behaviour of the model under a particular loading, just by looking at the fringe pattern. The screen with the grid lines can be rotated at different angles for the determination of slopes in different directions. The slope so obtained is, then, used for the determination of all other unknowns for the model.

For example, if the grid lines are parallel to the Y-axis of the model, we can obtain the values of bending moment, torsion and shear as follows:

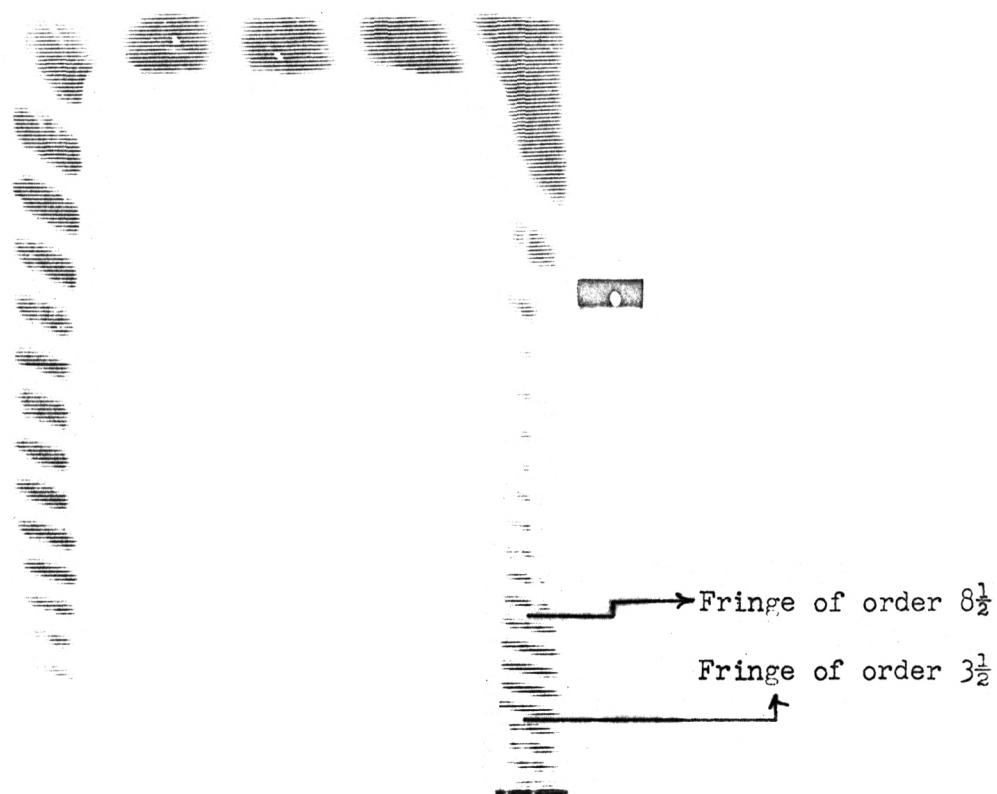
If slope = $\phi = k_x$,

$$M_x = EI_x K_{xx},$$

$$T_x = GJ_x K_{xy},$$

and $F_x = EI_x K_{xxx}$.

A sample fringe pattern is shown in Fig. 3. The pattern will give the values of bending moment in the beams AC and BD by the measurement of fringe spacings along their centre-lines. Similarly, the measurement of the fringe-spacings on the beam CD will give the values of torsion, as the grid lines run parallel to its centre-lines. The values of shearing forces can, then, be found from the corresponding values of the bending moments.



Sample Fringe pattern

Fig. 3

EQUIPMENT AND TEST PROCEDURE

Equipment

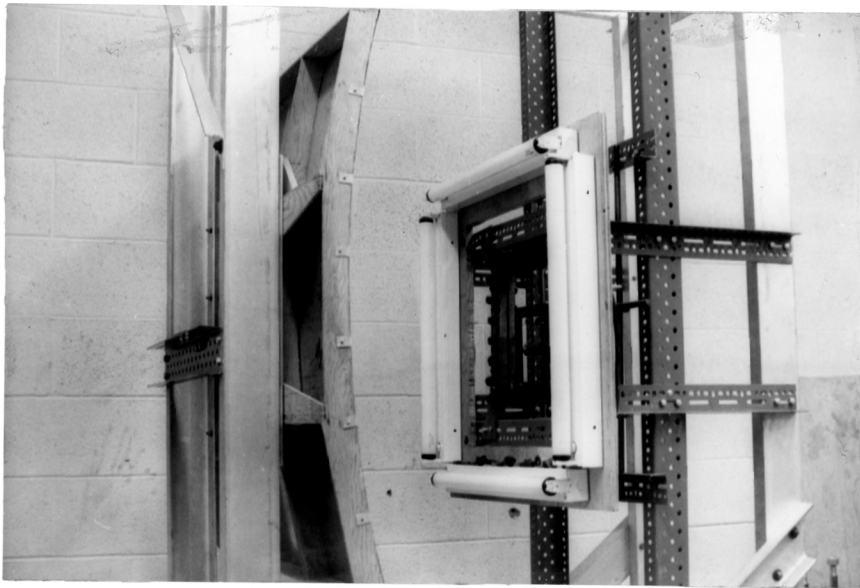
The test equipment consists, essentially, of the following parts:

- (a) Screen with the required illumination,
- (b) Photographic setup,
- (c) Model supports,
- (d) Loading arrangement,
- (e) Black plexiglas model of test structure.

The above parts are held together and supported by a metal frame, made up of channels and angles, bolted together. The distance a , between the model surface and the grid surface is kept equal to 24-in., which is $\frac{1}{3.5}$ times the radius of the cylindrical screen. The general setup of the apparatus is shown in Fig. 4.

The Screen. The grid paper was specially printed by the University Press on the KSU campus for this purpose, with a line width of 1/24" (or d , the spacing between the grid lines = 1/12"). The grid spacing was kept 1/12" throughout the tests on the basis of the recommendations of Kubitz (10), who observed that the fringes were difficult to locate for closer spacings; while on the other hand, for larger spacings, there is less accuracy.

The sheets of papers containing the grid lines were then pasted on the aluminum screen which has a cylindrical surface with a radius R equal to 3.5 times the distance between the model surface and the grid surface. The screen can be rotated about its axis on an aluminum ring through any desired angle, by loosening four wingnuts at the back. The grid was illuminated by four 20 watt fluorescent tubes 23" long, mounted on a



Moiré Fringe apparatus

Fig. 4

plywood frame, fixed around the model frame, which provided quite uniform illumination of the screen rulings in any rotational position.

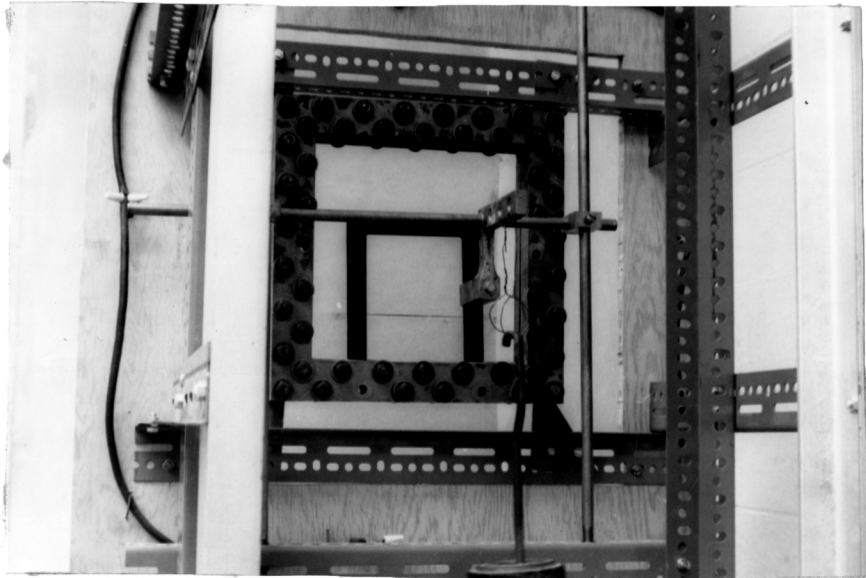
Photographic Setup. A 35 m.m. Leica camera, with a High Contrast copy film, was used for all the photographs. The combination yielded sharp negatives with a good contrast between the dark and light fringes. The enlargements obtained from these negatives were also found to be quite good, with a clear definition of the half fringes and the integer fringes. The camera was rigidly mounted on a steel plate behind the tiny hole in the centre of the grid.

Model Supports. The model was supported in a vertical position in a square steel two part frame. The two pieces were held together by numerous bolts, with the model supports placed in between the frame halves and the bolts tightened to achieve a built in condition at the supports of the model.

Loading Arrangement. The load was applied with the aid of a lever arrangement which could transform a vertically suspended weight into a horizontal load, perpendicular to the model surface. The load could be applied at any part of the model by moving the lever to any horizontal and vertical position required. Level measurements were made to ensure that the load was always acting perpendicular to the model surface.

The details of the loading arrangement and the model supports are shown in Fig. 5.

The Model. All of the models were made of black plexiglas, $1/4$ " thick, with a very good reflecting surface. The thickness of the plexiglas sheet was checked at different points with the help of a micrometer screwgauge and the model was cut from a portion of the sheet with the nearly uniform



Details of loading arrangement and model supports

Fig. 5

thickness. The thickness variation was around 5% in most of the cases.

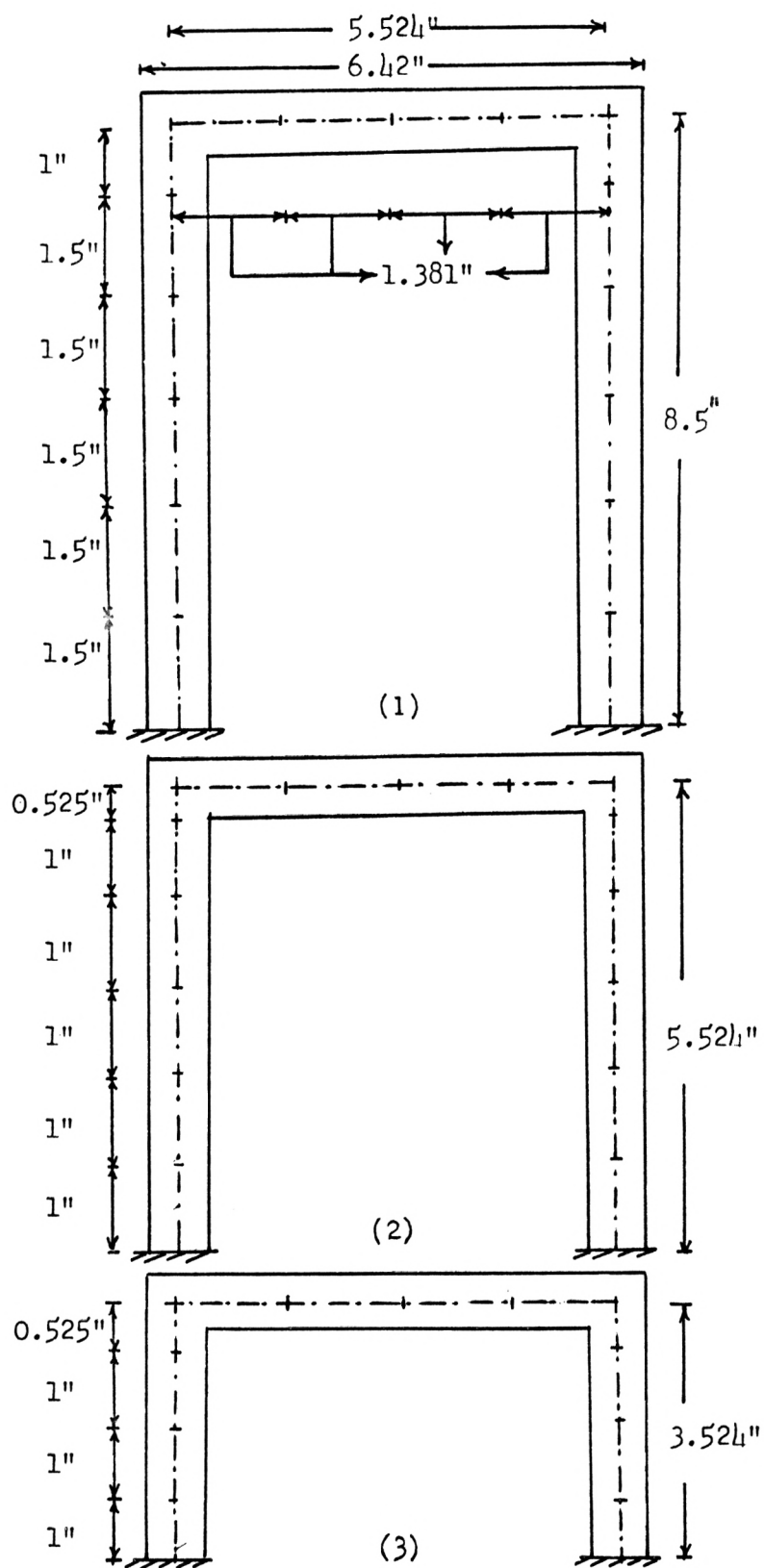
Test Procedure

In all, five models were tested. The first two models were used to obtain, experimentally, the proper exposure time which would give a set of sharp fringes, and to check the experimental setup. For the latter, a fixed beam model was used, and the experimental results were verified by the known theoretical results. The close agreement indicated that the apparatus and the general setup were operating correctly. A frame model was then tested as a prelude to the actual work. The other three models were of rectangular balcony girder frames on which the actual detailed experimental and analytical analyses were carried out, and only the results of these models are presented here.

All of the models were prepared by, first, roughly sawing out a piece of plexiglas slightly larger than the actual model with the aid of a saber saw, and then bringing it to the proper size and shape by the use of a plastic model-making machine with a vertical rotating cutter.

The shapes and the sizes of the three models are shown in Fig. 6. It will be noticed that the width of the models was kept constant in all the three cases, while the height was changed. The height was made greater than the width in model no. (1), equal to the width in model no. (2), and less than the width in model no. (3). This was done in order to observe the effect of a change of the ratio of height to width on the bending moment, torsional moment and shearing force in the model.

Fifteen load positions were tried for models (1) and (2) and eleven for (3). The models were loaded along their center-lines to obtain a



Models with their load positions

Fig. 6

sufficient number of points for drawing the bending moment, torsional moment, and shear force influence lines. The load positions are shown in Fig. 6. For each load position, two sets of photographs were taken, one with the grid lines horizontal to get the bending moment and shear force in the legs and torsional moment in the beam, and the second with the grid lines vertical to obtain the values of bending moment and shear force in the beam and torsional moment in the legs. For each set i.e. for each position of the grid lines, two exposures were taken, first for the unloaded state and the second for the loaded state which was superimposed on the first one.

A one pound load was first used for all the load positions, but it was found that the number of fringes per unit length was not sufficient to give an accurate result for load positions near the fixed supports. Higher loads were therefore used for load positions near the supports.

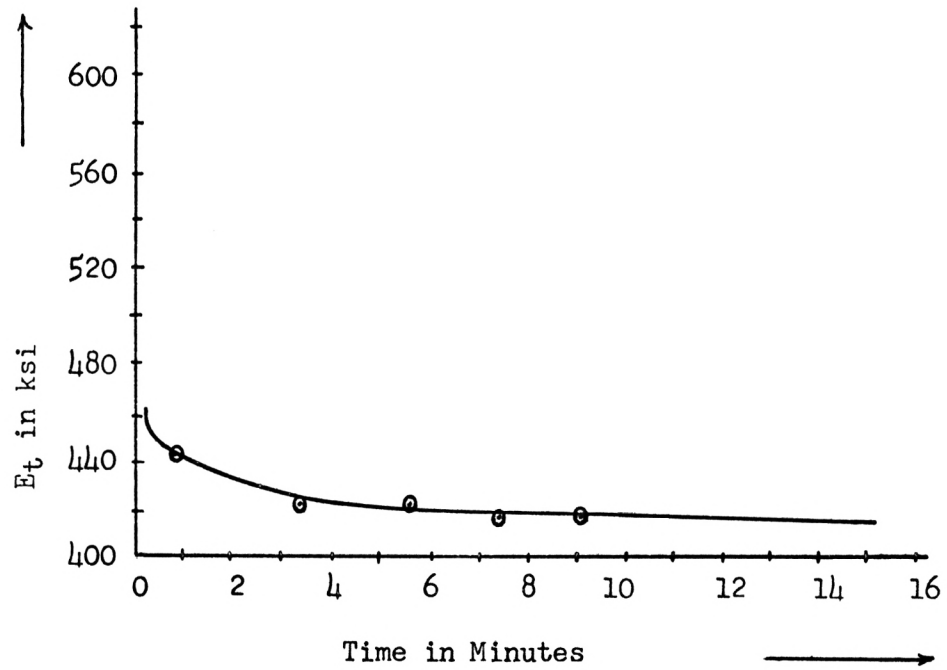
TESTING SEQUENCE AND DETERMINATION OF TIME DEPENDENT MODULUS, E_t

Testing Sequence

The value of the modulus of elasticity is a function of time for plexiglas, as it is a visco-elastic material. Carpenter has shown that about 80% of the variation in the value of E takes place in the first three or four minutes of the load application (10). Kubitza has also verified his results by using an L-shaped cantilever beam subjected to a concentrated load for 10 seconds, 1.5 minutes, 4.5 minutes and 10 minutes (10). He determined the corresponding values of E_t by equating the known theoretical slope with the slope obtained from the fringe photographs. His results are shown in Fig. 7, which gives a good idea of the variation of E_t with time.

From the above, it is quite clear that the time element is very important in experiments with plexiglas models. A definite time sequence is, therefore, necessary. On the basis of the results of Kubitza and Carpenter, a particular time sequence was chosen and used throughout the experimental work. The time of exposure was determined on the basis of many preliminary tests, and $11\frac{1}{2}$ seconds was finally adopted as the exposure time for all the photographs as it yielded best photographs of the fringe pattern. The complete time sequence used for the tests is given below:

Each exposure was made for $11\frac{1}{2}$ seconds as mentioned above. The first exposure was made after $4\frac{1}{2}$ minutes had passed since removing the previous load. The load was, then, applied using the lever arrangement, which took about 20 seconds. The load was kept acting for $4\frac{1}{2}$ minutes, and the second exposure of $11\frac{1}{2}$ seconds was, then, superimposed on the first exposure,



Variation of E_t with time for plexiglas (10)

Fig. 7

and the load was removed.

Determination of the Value of E_t

The values of E_t , corresponding to $4\frac{1}{2}$ minutes time of application of load on the plexiglas models was determined by using a model of a simply supported beam, cut from the same portion of the plexiglas sheet from which the test models were taken. The beam was then placed on two simple supports and a concentrated load was applied in the form of a weight suspended at the center of the beam. A dial gauge was used for the determination of the deflection of the beam at the centre for that load, applied for $4\frac{1}{2}$ minutes. The value of E_t was then calculated using the following deflection formula,

$$\text{Deflection } \delta = \frac{WL^3}{48EI} ,$$

where W = load applied at the centre of the beam,

δ = deflection at the centre, measured by the dialgauge,

I = moment of inertia of the beam section,

and L = the span of the simply supported beam.

$$\therefore E_t = \frac{WL^3}{48\delta I}$$

The observations and the values of δ obtained for each observation are given in the table below.

Experimental Determination of E_t for 4.5 minutes
time of application of load

- (i) $W = 1 \text{ Lb.}$
(ii) Least Count of the dial gauge = 0.0001"
(iii) Determination of δ :

TABLE NO. 1

S. No.	Deflection measurement by dial gauge			δ
	Initial dial reading	Final dial reading	Difference	in inches
1	12	68	56	0.0056
2	11	70	59	0.0059
3	10	57	47	0.0047
4	4	59	55	0.0055
5	10	64	54	0.0054
6	6	60	54	0.0054
7	2	60	58	0.0058
8	8	63	55	0.0055
9	12	61	59	0.0059
10	9	63	54	0.0054
11	10	64	54	0.0054

Mean = 0.0055

$$E_t = \frac{WL^3}{48\delta I} = \frac{1 \times 5^3}{48 \times 0.0055 \times 0.0011}$$

$$= \underline{430,000 \text{ psi}}$$

This is in very good agreement with the value obtained by Kubitza (10). His value of $E_t = 425 \text{ ksi}$ was used for the analysis of model no. 1, while the value of $E_t = 430 \text{ ksi}$, as obtained above, was used for the rest of the models.

GENERAL CHARACTERISTICS OF FRINGE PATTERNS

Before proceeding further, it is deemed necessary to deal in brief with what a fringe pattern actually represents qualitatively and what information it provides in a general sense without making any calculations. In fact, a fringe photograph is not only a complete record of the slope of the model at different points in the direction perpendicular to the grid lines, but it also indicates the general distribution of bending moments, shearforces, and torsional moments in that direction. Therefore, one can have a general idea about the distribution of stresses in the model just by looking at the fringe photograph.

A fringe photograph will indicate the following characteristics to a knowledgeable observer:

(1) Fringes perpendicular to the grid lines indicate the presence of torsion without bending moment in the element.

(2) Fringes parallel to the grid lines indicate the presence of bending moment without torsion in the element.

(3) Fringes inclined to the grid lines indicate the presence of bending moment and torsion. The degree of inclination indicates the ratio of the two.

(4) Equidistant fringes indicate a constant bending moment or torsional moment.

(5) Increase in fringe spacing indicates a decrease in bending or torsional moment.

(6) A change of direction of the fringes indicates a change of sign in bending or torsional moment.

PRESENTATION AND EVALUATION OF EXPERIMENTAL RESULTS

As already mentioned, several load positions were used for each model in order to get enough points to draw the influence lines. Fifteen load positions were used for models number 1 and 2, and eleven for model number 3. Two photographs were taken for each load position; one with the grid lines horizontal or in other words perpendicular to the legs. This photograph gave the torsional moment in the beam and the bending moment in the legs. The second photograph was taken with the grid lines vertical, and gave the bending moment in the beam and the torsional moment in the legs. A total of 82 photographs were taken.

The photographs obtained were in general quite satisfactory, with many of them having sharp fringes. Some of them, however, had dim fringes on one of the legs, making it very difficult and in some cases impossible to measure the fringe spacings. One other difficulty faced in analyzing some of the photographs was that the number of fringes per unit length on the beam was not large enough for a complete analysis of the beam. This might have been not only because of the smaller width of the beam, but perhaps also because the bending moment changed sign in the beam, so that the fringes also changed direction in the small width. Heavier loads could have been used in order to increase the number of fringes on the beam, but they would have increased the number of fringes on the legs to such an extent, that it would have become almost impossible to measure their spacings.

In reducing the data from the fringe patterns to determine the curvatures and rotations, a semi-graphical procedure was followed in this study. Enlargements in 5" x 4" size were first obtained from the negatives. Fringe

spacings were then measured directly on the photographs and were multiplied by the scale factor to obtain the actual fringe spacings. Slope curves were plotted between the fringe order and the distance, for each member of the frame. From these curves, bending and torsional moments were directly obtained as shown in the sample calculations below, and the bending moment, shear force and the torsional moment diagrams were then plotted.

A complete sample evaluation of results follows for model number 1, with the load at station 5. Analyses for other load positions and other models were carried out in a similar way and the final experimental results are shown in a tabular form at the end of this chapter.

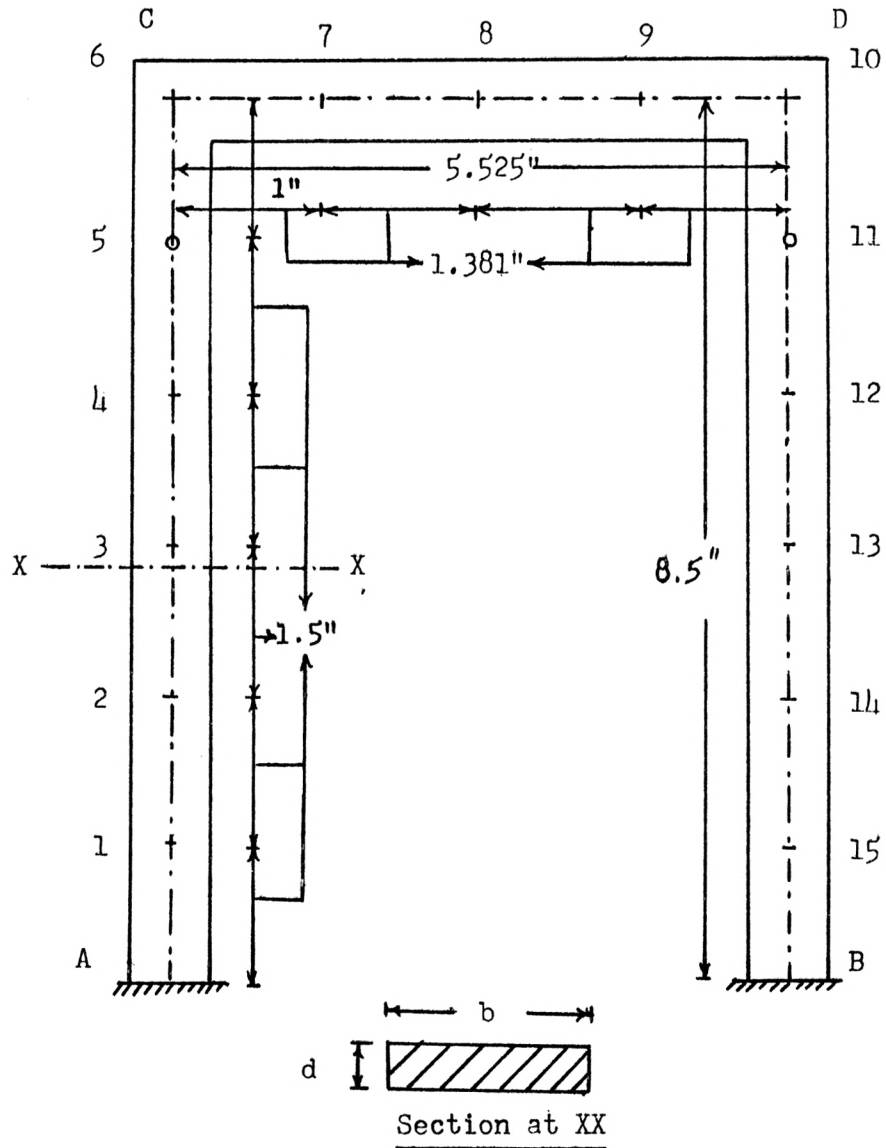
Sample Evaluation of Results

Fig. 8 shows the model with all the dimensions and the load positions. It should be noted that load positions 5 and 11 are symmetrically placed and therefore the value of bending moment and torsional moment at any point in the leg AC with the load at station 11 is equal to the bending moment or torsional moment at the corresponding point in the leg BD, with the load at station 5. The analysis was therefore carried out sometimes using the photographs for load at station 5 and sometimes using the photographs for load at station 11, whichever was convenient and whichever gave the sharpest fringes for the member under consideration.

The analysis was carried out as follows.

(I) Bending Moment and Shear Force

The fundamental equation for the bending moment $M = EI \frac{d^2y}{dx^2}$ can be



Width, $b = 0.897"$

Depth, $d = 0.243"$

Moment of inertia, $I_{yy} = 0.0011 \text{ In}^4$

Polar moment of inertia, $J_p = 0.00352 \text{ In}^4$

Model No. 1

(Load at sta. 5 or 11)

Fig. 8

expressed in difference form as

$$M_y = EI \frac{\Delta K_y}{\Delta y} ,$$

where,

ΔK_y = change in slope in the Y-direction,

and Δy = change in distance in the Y-direction.

But, $\Delta K_y = n \times (\text{change in slope per fringe order})$

$$= n \frac{\Delta \phi}{\Delta y} = n \frac{d}{2a}$$

where,

n = fringe order,

d = fringe spacing = $1/12''$,

and a = distance between the model and the screen.

Therefore, choosing $n = 2$ i.e. considering two fringe spacings, we obtain

$$\Delta K_y = \frac{2 \times 1/12}{2 \times 24} = \frac{1}{288}$$

$$\text{As } I = \frac{bd^3}{12} = \frac{0.897 \times (0.243)^3}{12} = 0.0011 \text{ in}^4$$

and $E = 430,000 \text{ lbs./in}^2$, for $t = 4.5$ minutes, as determined experimentally,

$$\begin{aligned} M_y &= EI \frac{\Delta K_y}{\Delta y} = \frac{430,000 \times 0.0011 \times 1/288}{\Delta y} \\ &= \frac{1.646}{\Delta y} , \text{ for } t = 4.5 \text{ minutes} . \end{aligned}$$

-----Eqn. (1)

(a) Determination of bending moment and shear force in leg AC with the load at station 5, or in leg BD with the load at station 11.

As already explained, for the determination of bending moment in a member of the frame, the photographs with the gridlines perpendicular to the centre line of that member were used. Therefore, for the determination of bending moment in AC or BD, the photograph with the grid lines horizontal were used.

The photographs, with the grid lines horizontal and the load first at station 5 and then at station 11 are shown in Figs. (9a) and (9b). With the load at station 5, the fringes are not clear on all of leg AC. Therefore, the fringes on the leg BD with the load at station 11 have been used here.

The fringe spacings and the distance of every fringe from the fixed end were measured accurately for the leg BD on the photograph for the load at station 11, and were then multiplied by the scale factor to get the actual spacings and the distances. A curve was then plotted of the fringe order versus the distance from the fixed end and is shown in Fig. 10.

The values of bending moments were then calculated at a number of fringe positions from the fringe order versus distance curve using equation (1).

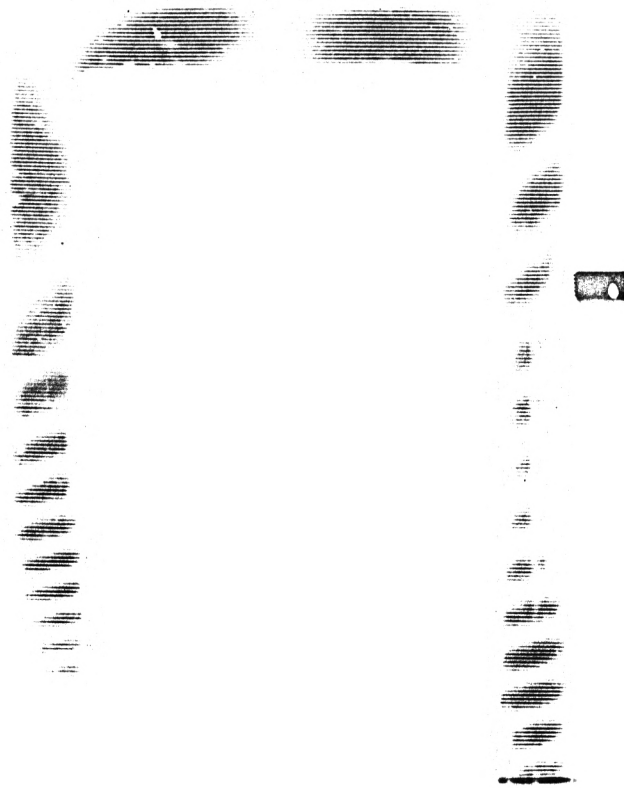
For example, taking the fringe order equal to 7.5,

$$\begin{aligned}\Delta y &= \text{distance between the fringes of order 6.5 and 8.5} \\ &= 0.57", \text{ as shown in Fig. 10.}\end{aligned}$$

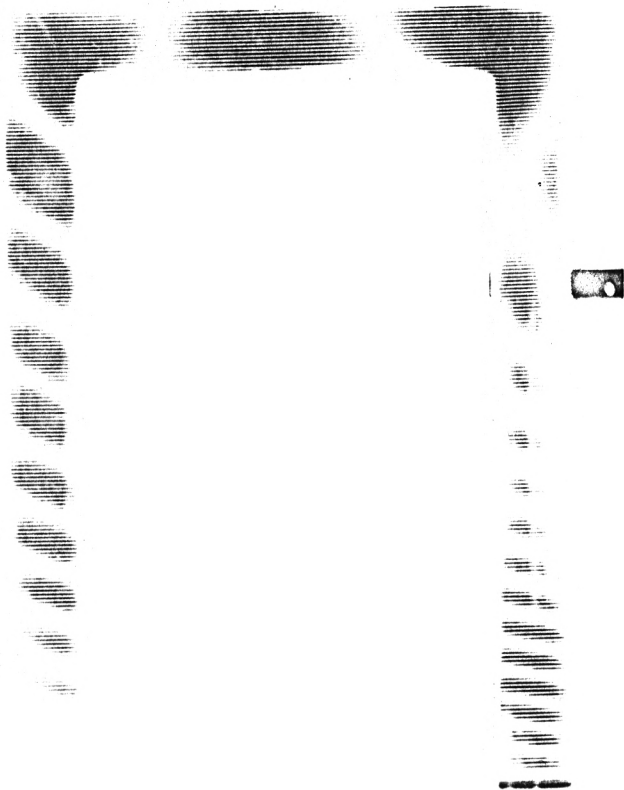
Therefore, using equation (1), we obtain

$$M_y = \frac{1.646}{\Delta y} = \frac{1.646}{0.57} = 2.90 \text{ In. Lbs.}$$

As the distance of the 7.5 order fringe was 2.2" from the fixed end A, the co-ordinates of the point P, so obtained, are (2.9, 2.2) on the bending



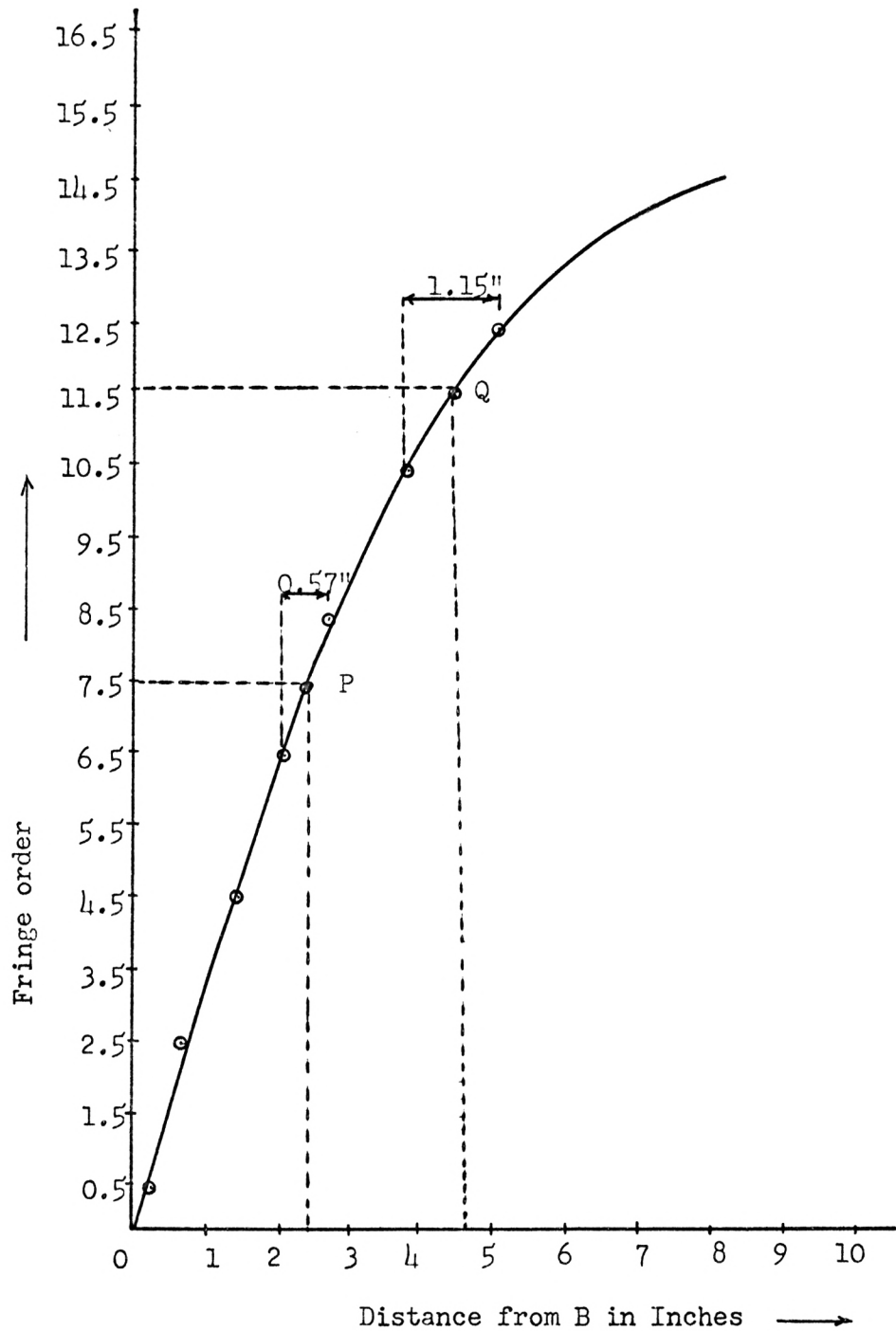
(a) Load at sta. 5



(b) Load at sta. 11

Fringe photographs with grid lines horizontal

Fig. 9



Fringe order versus distance curve for leg AC with
load at sta. 5

Fig. 10

moment diagram.

Similarly, for obtaining the point Q on the bending moment diagram, the fringe of order equal to 11.5 was used, which is at 4.3" from the end and for which $\Delta y = 1.15$ ". We, therefore, get the bending moment

$$M_y = \frac{1.646}{\Delta y} = \frac{1.646}{1.15} = 1.43 \text{ In. Lbs.}$$

In a similar way, bending moments for many points were calculated and the bending moment diagram was drawn for the leg BD with the load at station 11 which is also the bending moment diagram for the leg AC with the load at station 5. The bending moment diagram is shown in Fig. 11. With the help of the bending moment diagram, the shear force diagram can be plotted. Since the bending moment is varying linearly, the shear force will be constant and will be equal to the rate of change of the bending moment.

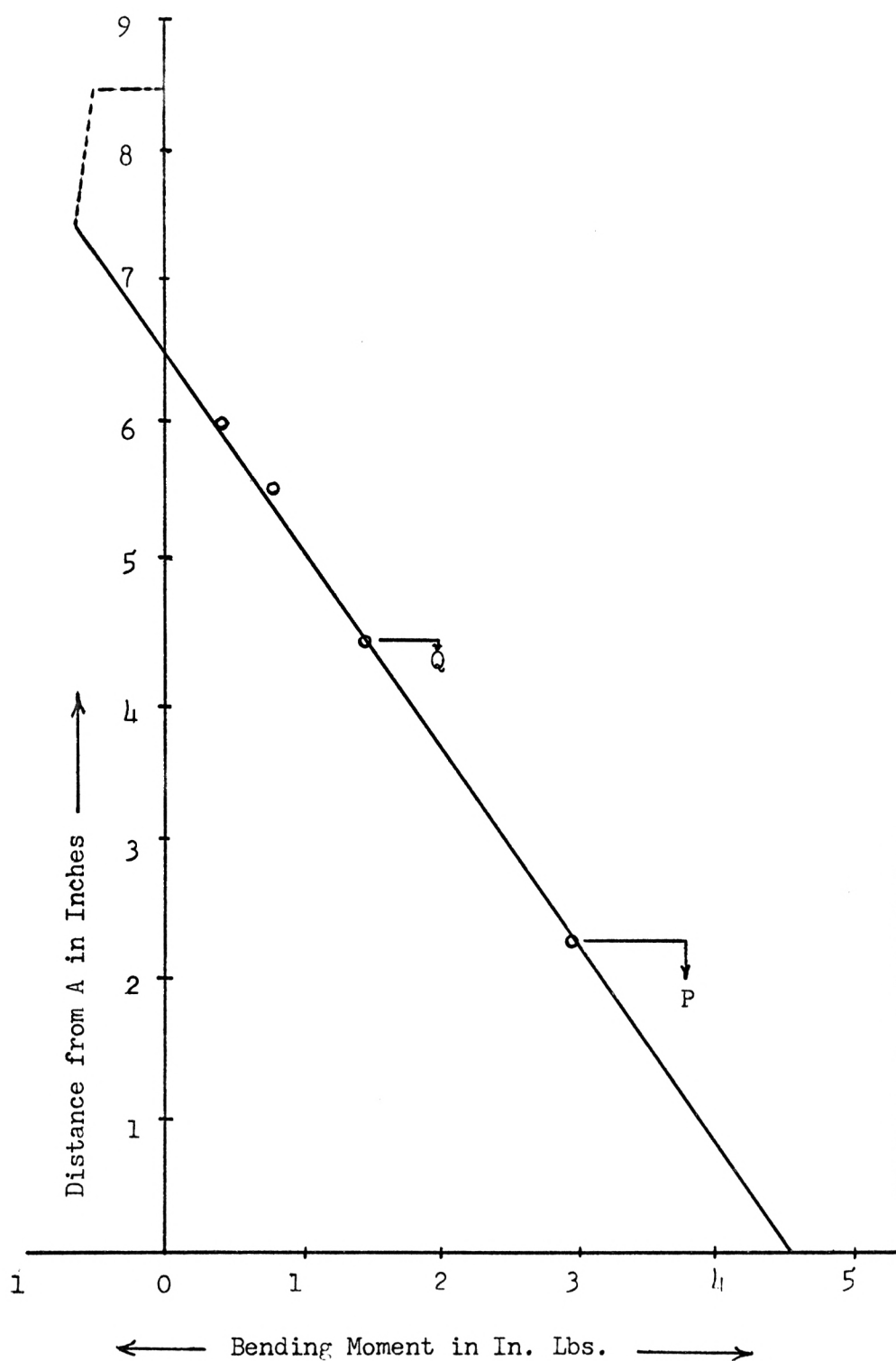
$$\begin{aligned} \text{Shear Force} &= \text{Rate of change of bending moment} \\ &= \frac{\text{Bending moment at P} - \text{Bending moment at Q}}{\text{Distance between P and Q}} \\ &= \frac{2.90 - 1.43}{4.3 - 2.2} = 0.70 \text{ Lbs.} \end{aligned}$$

The Shear Force diagram is shown in Fig. 12.

(b) Determination of bending moment and shear force in leg BD with the load at station 5 or in leg AC with the load at station 11.

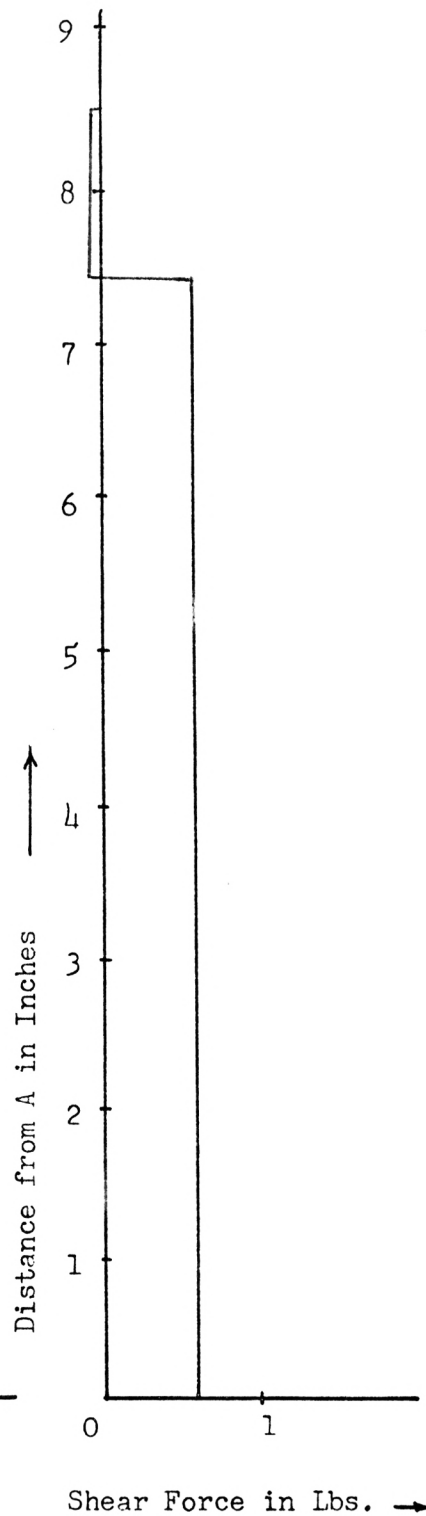
Here the photograph with the load at station 5 was used as it gives clear fringes for the whole leg BD. The fringe order versus distance curve was drawn in the same way as already explained, and is shown in Fig. 13.

Values of spacing Δy were then picked from this graph and used in Eqn. (1) to obtain the bending moments at different points. The bending



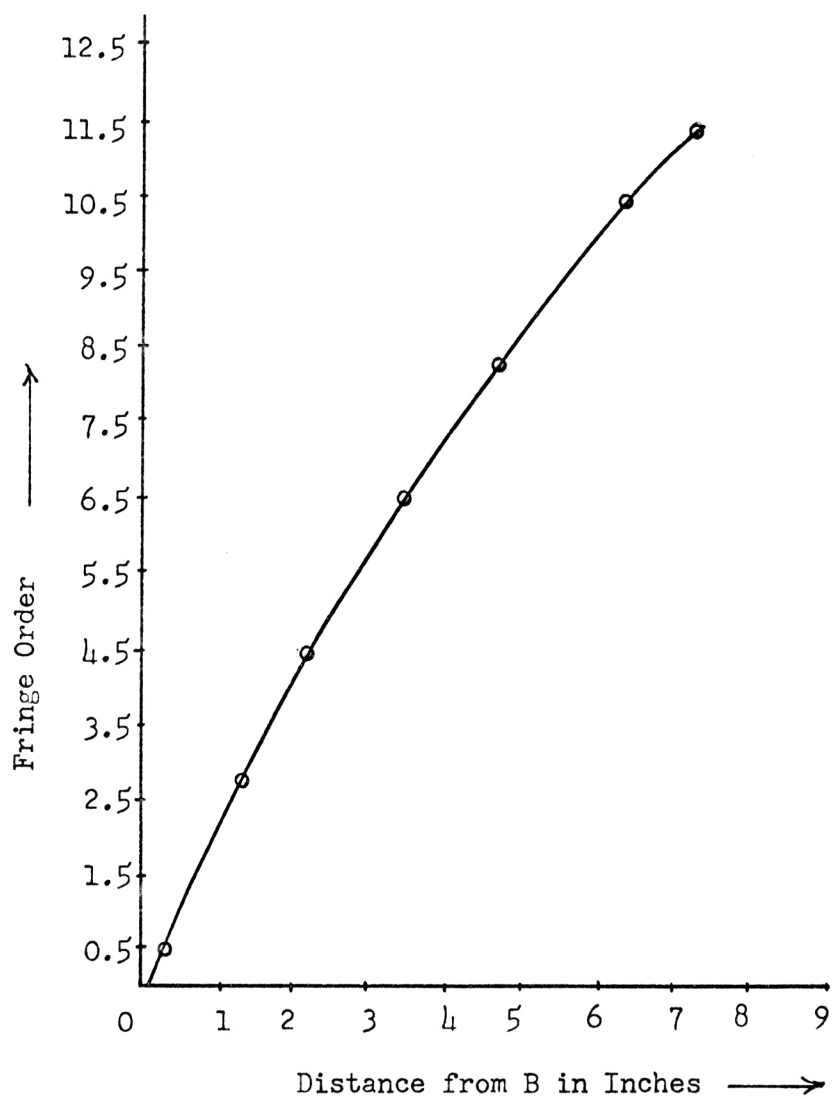
Bending Moment diagram for leg AC with
load at sta. 5

Fig. 11



Shear Force diagram for leg
AC with load at sta. 5

Fig. 12



Fringe order versus distance curve for leg BD with load at
sta. 5

Fig. 13

diagram was then drawn as for the other leg and is shown in Fig. 14. The Shear Force diagram was drawn by calculating the rate of change of bending moment from the bending moment diagram, and is shown in Fig. 15.

(c) Determination of bending moment and shear force in the beam CD for the load at station 5 or 11.

For the determination of bending moment in the beam, the photograph with the grid lines perpendicular to the beam (Fig. 16) was used. It has already been mentioned that the number of fringes on the beam was not large enough in some photographs. In this case, there were only three fringes on the whole beam which is the minimum number required for the analysis. The fringe order versus distance curve was drawn with the aid of these three fringes, and is shown in Fig. 17. Only two points were obtained from this curve for drawing the bending moment diagram, as shown in Fig. 18. The corresponding Shear Force diagram is shown in Fig. 19.

(II) Torsion.

(a) Calculation of the value of J_p , the polar moment of inertia for the rectangular section of the models.

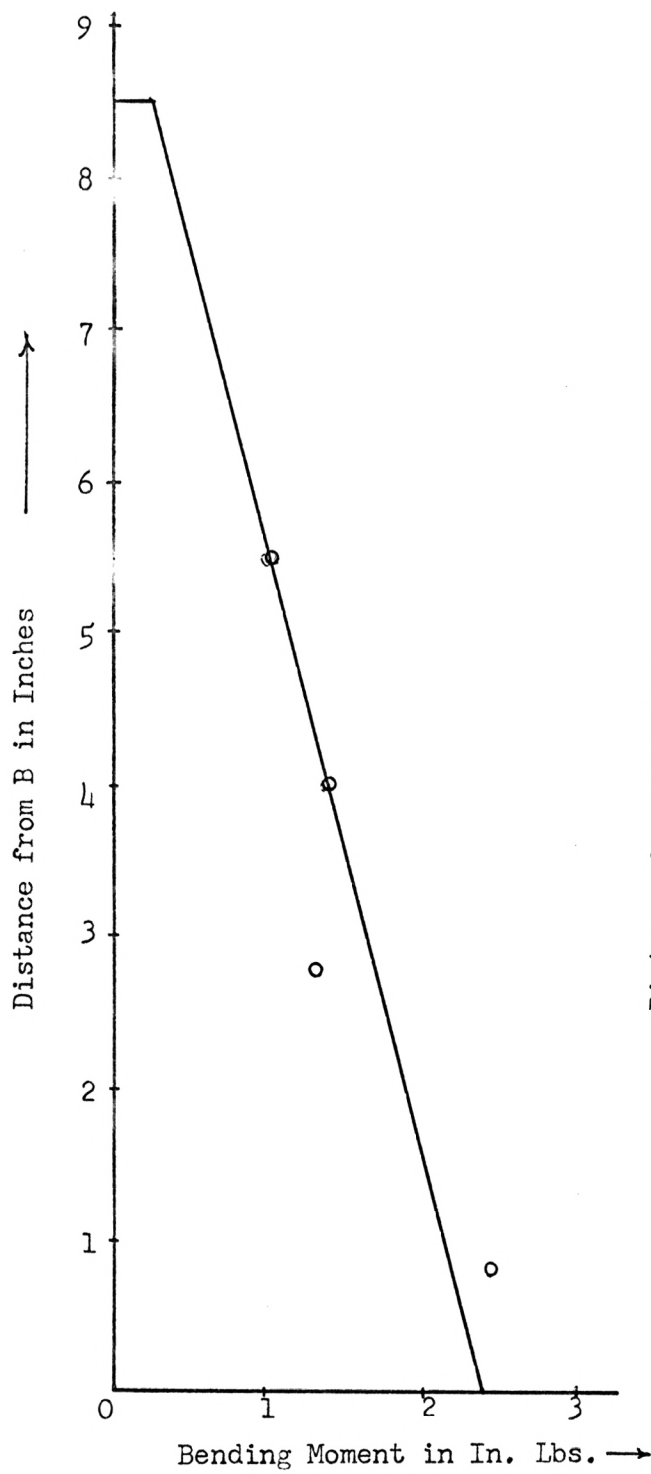
From Saint Venant's formula for a rectangular section, the polar moment of inertia, J_p , may be given by (29)

$$J_p = K_1 \frac{B^3 D^3}{B^2 + D^2}$$

where B = width of the cross section,

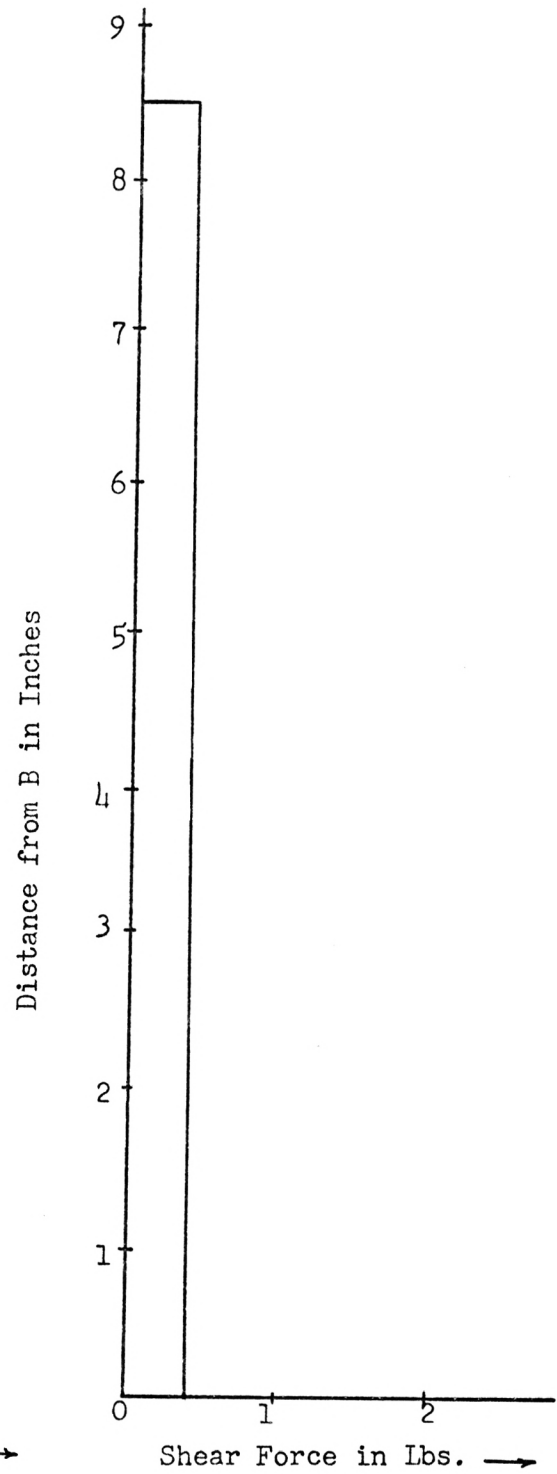
D = depth of the cross section,

and K_1 = a constant, given by



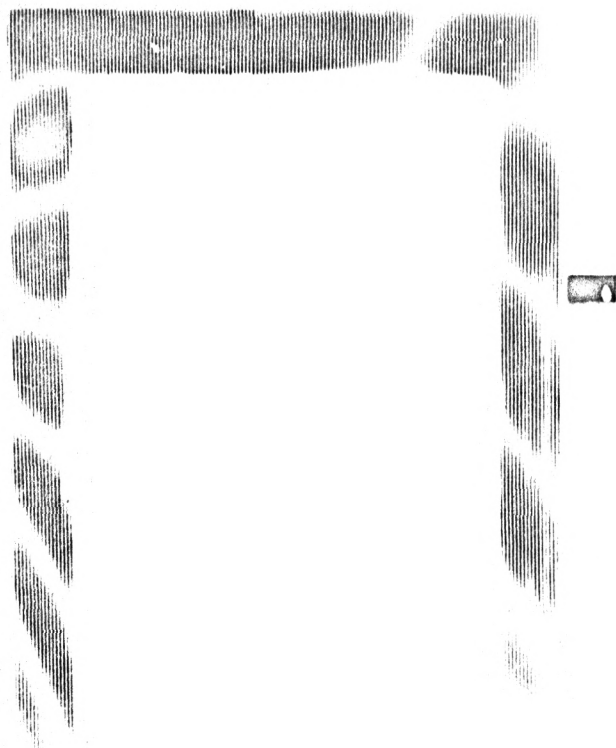
Bending Moment diagram for leg BD with load at sta. 5

Fig. 14

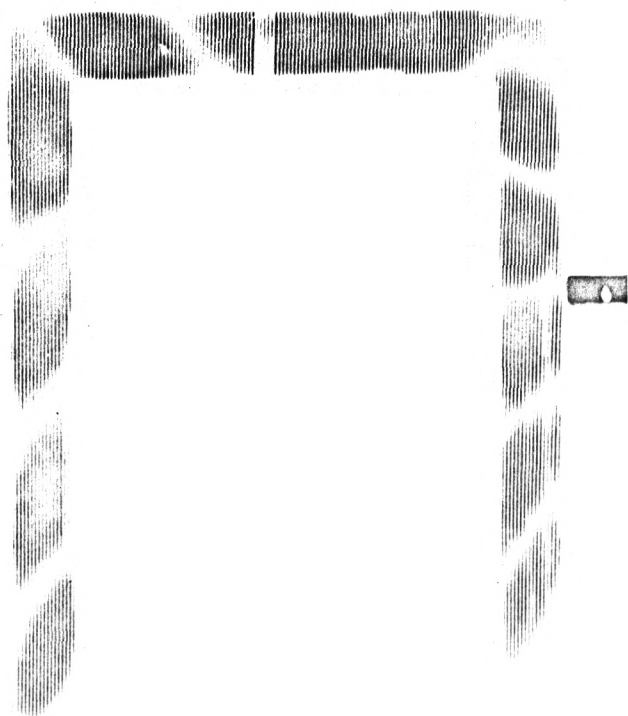


Shear Force diagram for leg BD with load at sta. 5

Fig. 15



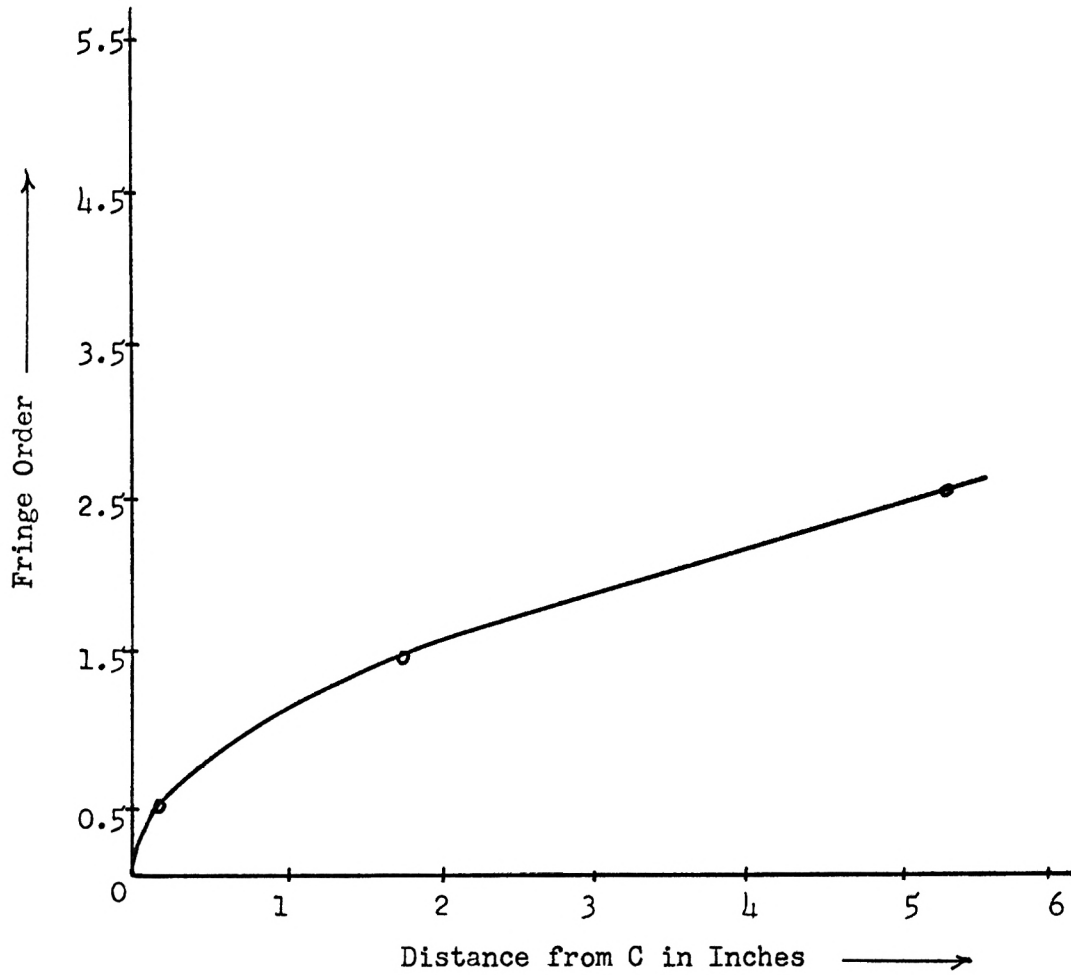
(a) Load at sta. 5



(b) Load at sta. 11

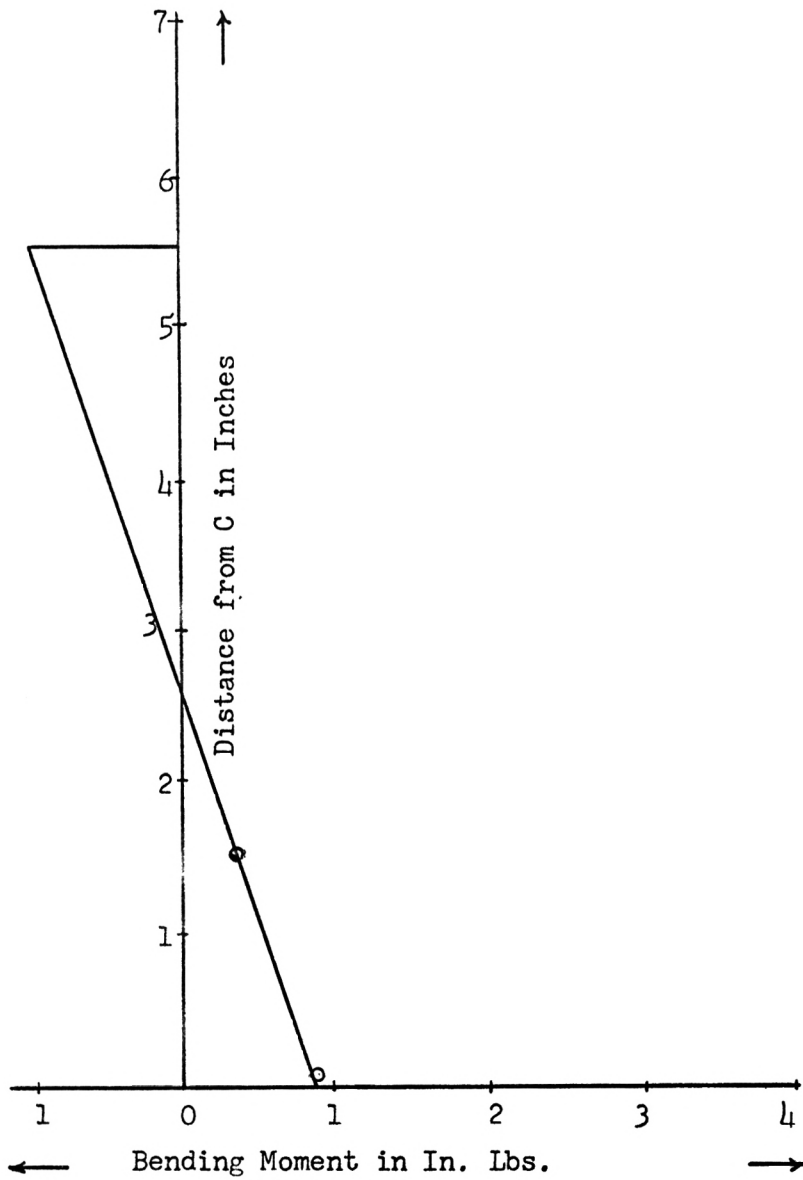
Fringe photographs with grid lines vertical

Fig. 16



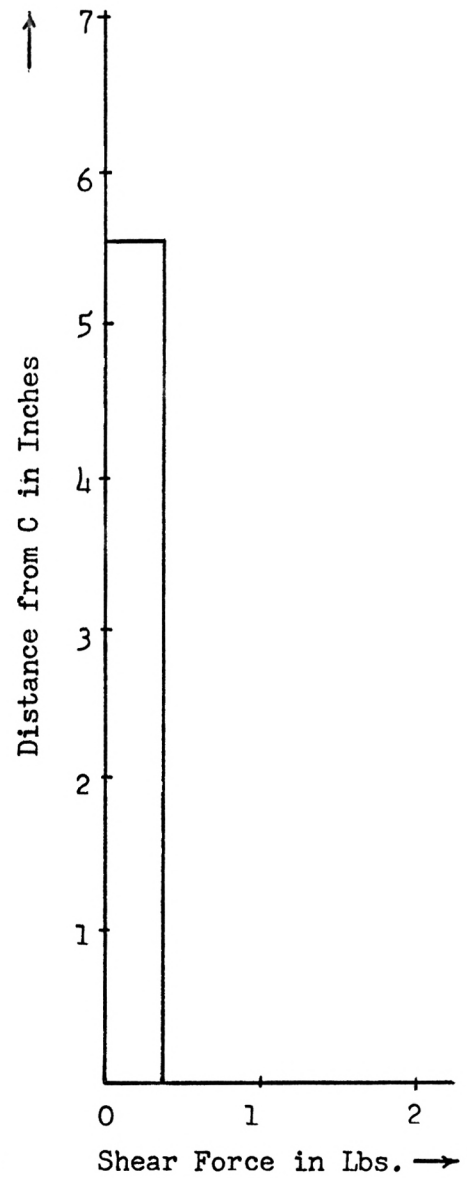
Fringe order versus distance curve for beam CD
with load at sta. 5

Fig. 17



Bending Moment diagram for beam CD with load at sta. 5

Fig. 18



Shear Force diagram for beam CD with load at sta. 5

Fig. 19

$$K_1 = \frac{1}{3.645 - 0.06 \frac{B}{D}} \quad .$$

Here, $B = 0.897''$ and $D = 0.243''$.

Therefore,

$$K_1 = \frac{1}{3.645 - 0.06 \frac{B}{D}} = \frac{1}{3.645 - 0.06 \times \frac{0.897}{0.243}}$$

$$= 0.292$$

$$\text{and } J_p = K_1 \frac{B^3 D^3}{B^2 + D^2} = \frac{0.292 \times (0.897)^3 \times (0.243)^3}{(0.897)^2 + (0.243)^2}$$

$$= \underline{0.00352} \text{ in}^4 \quad .$$

(b) Calculation of the value of G .

$$G = \frac{E}{2(1+\mu)} = \frac{430,000}{2(1+0.26)} = 170,800 \text{ psi}$$

(c) Determination of torsional moments

Torsional moment at any point along the centre line of a member is given by

$$T_y = GJ_p \frac{\Delta K_y}{\Delta y} \quad ,$$

where ΔK_y = change in the slope along the centre line

and Δy = change in the distance along the centre line.

$$\therefore T_y = GJ_p \frac{n \Delta \phi_y}{\Delta y}$$

$$= GJ_p \frac{n d / 2a}{\Delta y}$$

-----Equation (2)

$$\text{For } n = 2, T_y = \frac{170,800 \times 0.00352 \times 2 \times \frac{1/12}{2 \times 24}}{\Delta y}$$

$$= \frac{2.09}{\Delta y} \quad \text{-----Equation (3)}$$

(i) Determination of torsional moment in the leg AC.

For the determination of torsional moment in the legs, the photographs with grid lines vertical were used. Using the photographs shown in Fig. 16, for the load at station 5, a graph was drawn of the fringe order versus the distance from the base of the leg. This graph plotted as a straight line showed that the torsional moment was constant in the leg.

From the graph, $\Delta y = 6.03''$, for $n = 4.5$. Therefore, using Eqn. (2), we obtain

$$\begin{aligned} \text{Torsional Moment} &= GJ_p \frac{n^2 a}{\Delta y} \\ &= \frac{170,800 \times 0.00352 \times 4.5 \times \frac{1/12}{2 \times 24}}{6.03} \\ &= 0.78 \text{ Inch Lbs.} \end{aligned}$$

The torsional moment diagram is shown in Fig. 21.

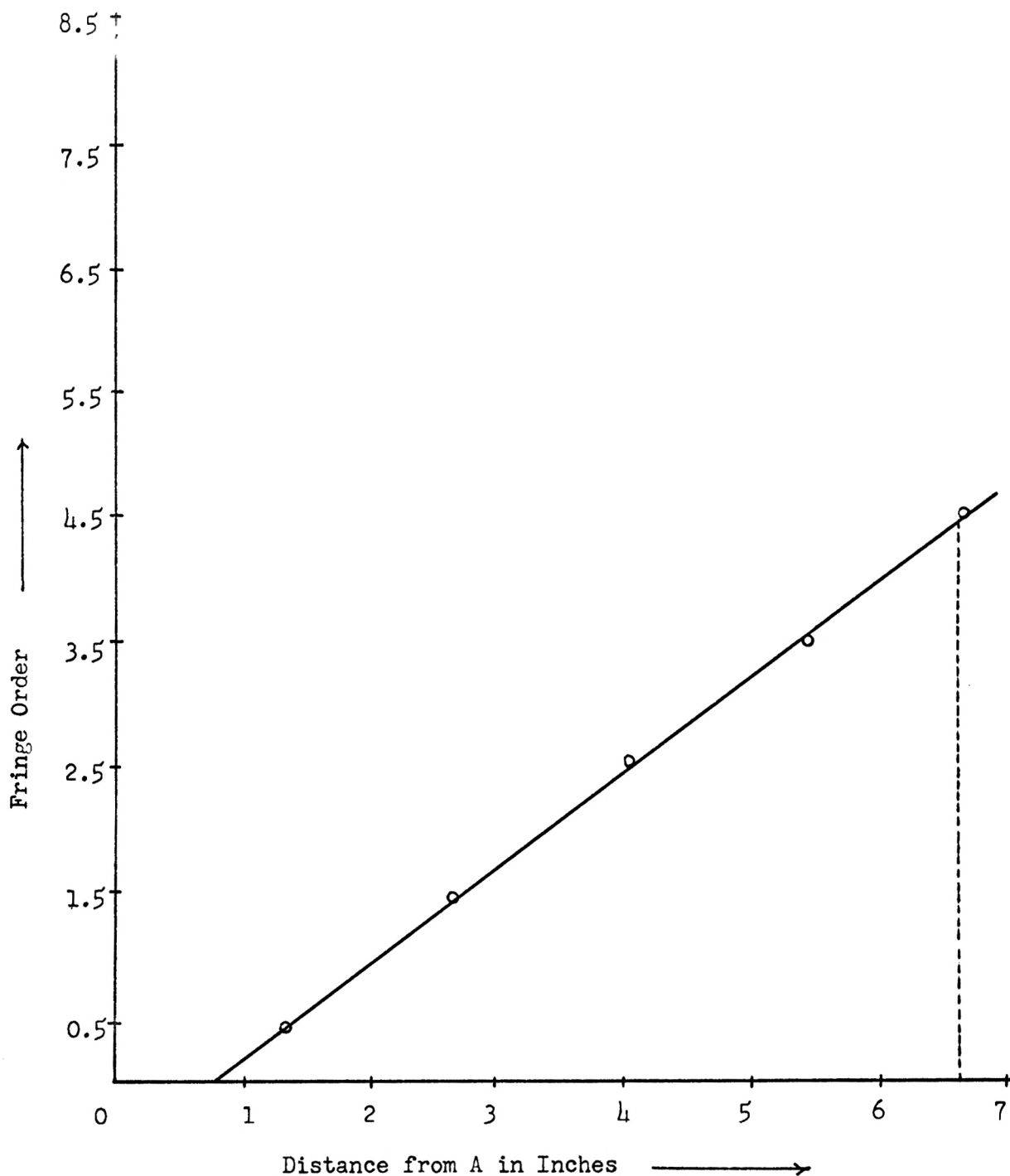
(ii) Determination of torsional moment in the leg BD

The torsional moment in the leg BD was found in a similar way and was the same as in AC.

(iii) Determination of the torsional moment in the beam CD.

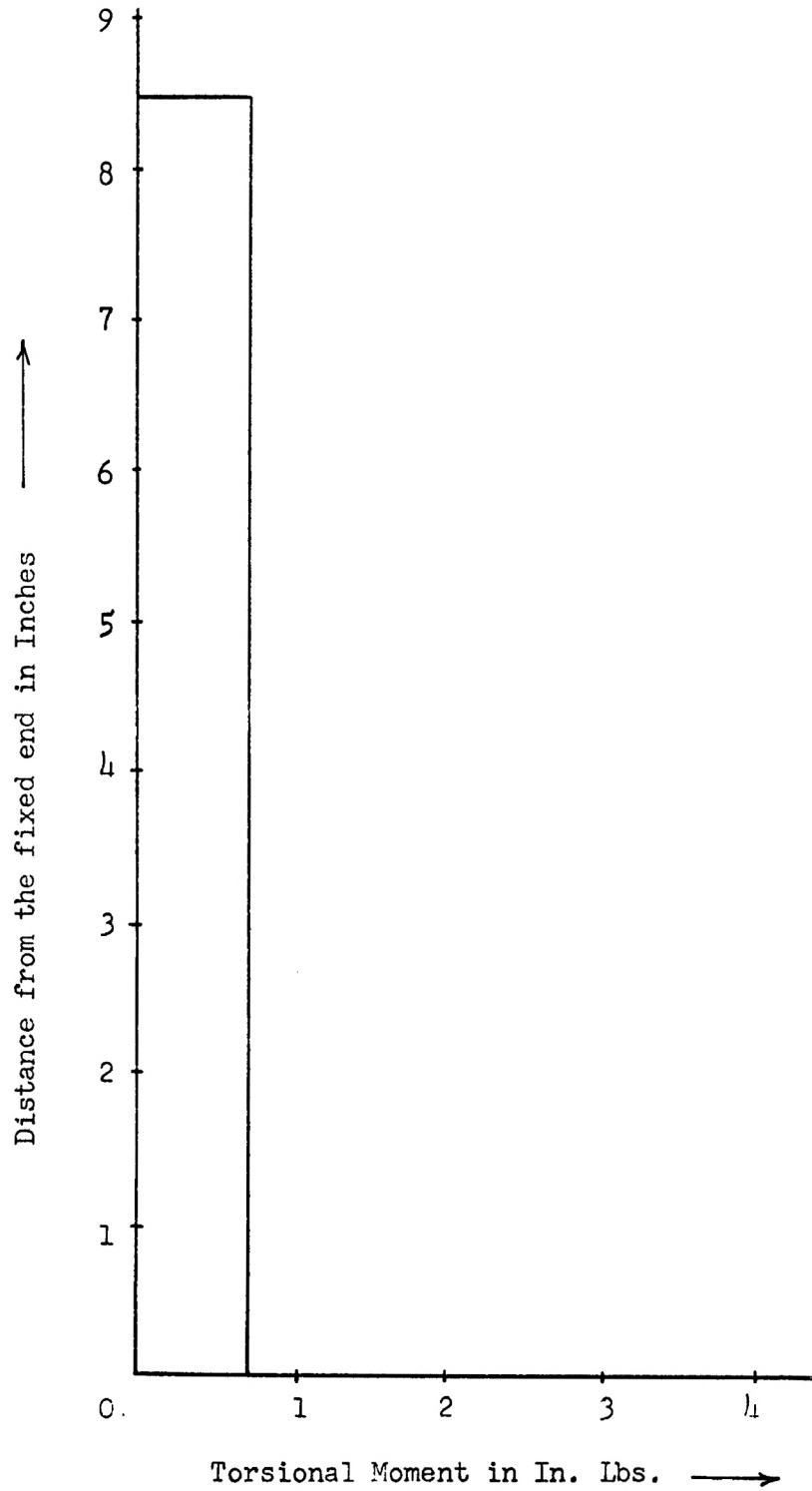
For the determination of torsional moment in the beam, the photograph with the grid lines horizontal (Fig. 9), was used. It had just three fringes on the beam and since the torsional moment was constant in the beam they were sufficient for the analysis. The distance between the first and the third fringe was measured and was equal to 4.86".

Therefore, for $n = 2$, $\Delta y = 4.86''$, using Eqn. (3), we obtain



Fringe order versus distance curve for leg AC with
load at sta. 5

Fig. 20

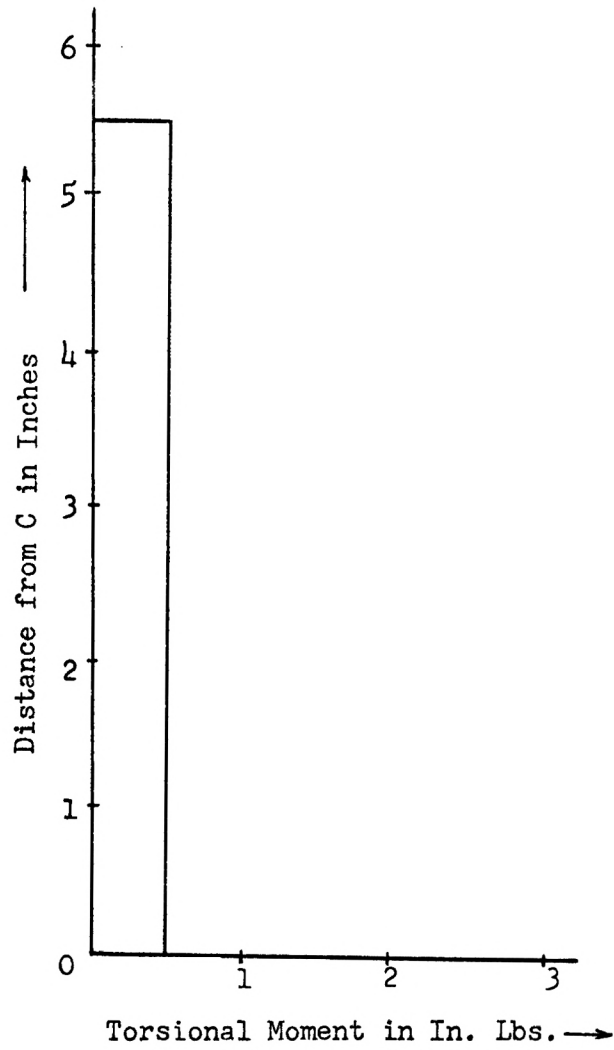


Torsional Moment diagram for leg AC or BD
with load at sta. 5

Fig. 21

$$\text{Torsion} = \frac{2.09}{4.86} = 0.43 \text{ Inch Lbs.}$$

The torsional moment diagram is shown in Fig. 22.



Torsional Moment diagram for beam CD with
load at sta. 5

Fig. 22

Final Experimental Results

Model No. 1

(Load W = 1 Lb., E = 425ksi)

TABLE NO. 2

Load at sta.	Shear Force at the fixed end B, F ₀ , in Lbs.	Bending Moment at the fixed end B, M ₀ , in In. Lbs.	Torsional Moment at the fixed end B, T ₀ , in In. Lbs.
1	--	--	--
2	--	0.545	--
3	0.1218	1.05	0.386
4	0.1706	1.50	0.535
5	0.2440	2.40	0.771
6	0.2460	2.69	0.803
7	0.400	3.50	0.450
8	0.492	4.18	--
9	0.600	4.68	--
10	0.687	5.23	-0.803
11	0.682	4.50	-0.771
12	0.702	3.30	-0.535
13	--	--	-0.386
14	0.903	2.350	--
15	--	--	--

Final Experimental Results

Model No. 2

(Load $W = 1.48$ Lbs., $E = 430$ ksi)

TABLE NO. 3

Load at sta.	Shear Force at the fixed end B, F_o , in Lbs.	Bending Moment at the fixed end B, M_o , in Inch Lbs.	Torsional Moment at the fixed end B, T_o , in Inch Lbs.
1	--	--	--
2	--	--	--
3	--	--	0.408
4	0.1795	1.310	0.597
5	0.280	2.050	--
6	0.275	2.30	0.824
7	0.414	2.882	0.613
8	0.691	3.80	0.445
9	0.956	4.590	0.00
10	1.046	4.810	-0.824
11	1.162	--	-0.723
12	1.232	4.190	-0.597
13	1.422	3.420	-0.408
14	--	--	--
15	--	--	--

Final Experimental Results

Model No. 3

(W = 1.48 Lbs., E = 430ksi)

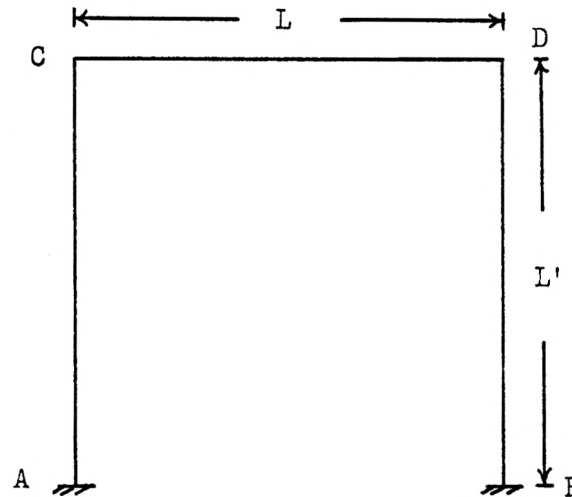
TABLE NO. 4

Load at sta.	Shear Force at the fixed end B, F_o , in Lbs.	Bending Moment at the fixed end B, M_o , in Inch Lbs.	Torsional Moment at the fixed end B, T_o , in Inch Lbs.
1	--	--	--
2	0.05	0.38	0.207
3	0.1361	0.813	0.336
4	0.1370	1.10	0.520
5	0.398	1.70	0.616
6	0.690	2.40	0.790
7	0.970	3.30	--
8	1.761	4.05	-0.52
9	--	--	--
10	--	--	-0.207
11	--	--	--

DEVELOPMENT OF THEORETICAL RESULTS
TO BE COMPARED WITH EXPERIMENTAL RESULTS

For the theoretical analysis of these frames, a set of equations was derived by using a strain energy method.

The figure below shows a rectangular balcony girder frame, rigidly built-in at A and B.



If the support B is removed, its effect can be replaced by a bending moment M_0 , a torque T_0 , and a shear force F_0 . These generalized forces were taken as the redundant elements in the derivation.

Hence, if U is the total strain energy of the beam, the conditions to be satisfied are

$$\frac{\partial U}{\partial M_0} = 0,$$

$$\frac{\partial U}{\partial T_0} = 0,$$

and $\frac{\partial U}{\partial F_0} = 0.$

The total strain energy of the beam is the sum of the components due to bending, torque and shear force. The strain energy due to the shear force is ordinarily much smaller than due to the other two and can consequently be neglected. Denoting the strain energy due to bending and torque by U_B and U_T respectively, we obtain

$$\frac{\partial U_B}{\partial M_0} + \frac{\partial U_T}{\partial M_0} = 0,$$

$$\frac{\partial U_B}{\partial T_0} + \frac{\partial U_T}{\partial T_0} = 0,$$

$$\frac{\partial U_B}{\partial F_0} + \frac{\partial U_T}{\partial F_0} = 0.$$

Given that ds is a small element anywhere along the length of the frame, EI is the flexural rigidity, and NJ is the torsional rigidity of the girder,

$$\text{then, } U_B = \frac{1}{2EI} \int M_x^2 ds, \quad U_T = \frac{1}{2NJ} \int T_x^2 ds.$$

M_x and T_x are the bending moment and the torsion at any section and the integration extends round the whole girder.

The above equations can, then, be re-written as

$$\frac{1}{EI} \int M_x \frac{\partial M_x}{\partial M_0} ds + \frac{1}{NJ} \int T_x \frac{\partial T_x}{\partial M_0} ds = 0, \quad \text{-----(a)}$$

$$\frac{1}{EI} \int M_x \frac{\partial M_x}{\partial T_0} ds + \frac{1}{NJ} \int T_x \frac{\partial T_x}{\partial T_0} ds = 0, \quad \text{-----(b)}$$

$$\frac{1}{EI} \int M_x \frac{\partial M_x}{\partial F_0} ds + \frac{1}{NJ} \int T_x \frac{\partial T_x}{\partial F_0} ds = 0 . \quad \text{-----}(c)$$

The sign convention used here is as follows:

- (a) a positive bending moment at X is one that tends to make dx convex upwards, when dx is viewed from the front.
- (b) a positive torque at X is one that tends to turn the viewed section clockwise, and
- (c) a positive shearing force at X is one that tends to raise the viewed section.

With these sign conventions, taking M_0 , T_0 , and F_0 as positive, we proceed as follows.

Load in CD

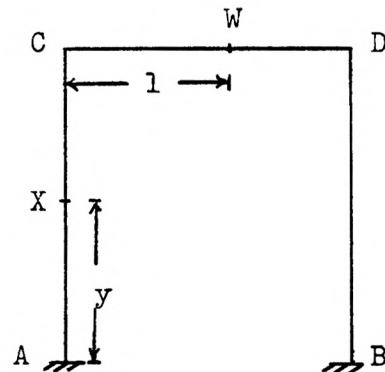
(I) Section in AC

M_0 imposes a bending moment = $-M_0$,

and a torsional moment = 0.

T_0 imposes a bending moment = 0,

and a torsional moment = $-T_0$.



$$M_x = -M_0 + 0 + F_0 y + W(L' - y) \quad \text{-----}(d)$$

$$T_x = 0 - T_0 + F_0 L - Wl \quad \text{-----}(e)$$

Therefore, from equations (d) and (e), we obtain

$$\frac{\partial M_x}{\partial M_0} = -1 \quad , \quad \frac{\partial T_x}{\partial M_0} = 0,$$

$$\frac{\partial M_x}{\partial T_0} = 0 \quad , \quad \frac{\partial T_x}{\partial T_0} = -1,$$

$$\frac{\partial M_x}{\partial F_0} = y \quad ,$$

$$\frac{\partial T_x}{\partial F_0} = L \quad .$$

(II) Section in CW

M_0 imposes a bending moment = 0, and a torsional moment = $-M_0$,

T_0 imposes a bending moment = T_0 , and a torsional moment = 0.

$$M_x = 0 + T_0 - F_0(L-x) + W(l-x) \text{ -----(f)}$$

$$\text{and } T_x = -M_0 + 0 + F_0L' - Wx_0 = -M_0 + F_0L' \text{ -----(g)}$$

From the above equations,

$$\frac{\partial M_x}{\partial M_0} = 0,$$

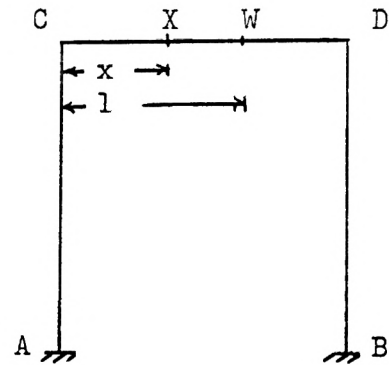
$$\frac{\partial T_x}{\partial M_0} = -1,$$

$$\frac{\partial M_x}{\partial T_0} = +1,$$

$$\frac{\partial T_x}{\partial T_0} = 0,$$

$$\frac{\partial M_x}{\partial F_0} = -(L-x),$$

$$\frac{\partial T_x}{\partial F_0} = L'.$$



(III) Section in WD

$$M_x = 0 + T_0 - F_0(L-x) + 0 = T_0 - F_0(L-x) \text{ -----(h)}$$

$$T_x = -M_0 + 0 + F_0L' + 0 = -M_0 + F_0L' \text{ -----(i)}$$

which give,

$$\frac{\partial M_x}{\partial M_0} = 0 \quad ,$$

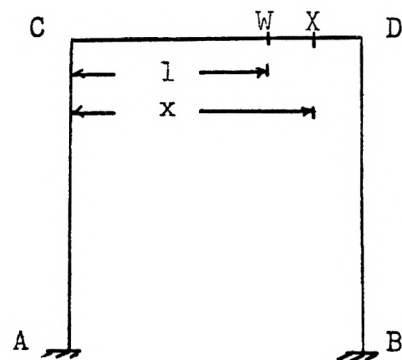
$$\frac{\partial T_x}{\partial M_0} = -1 \quad ,$$

$$\frac{\partial M_x}{\partial T_0} = +1 \quad ,$$

$$\frac{\partial T_x}{\partial T_0} = 0 \quad ,$$

$$\frac{\partial M_x}{\partial F_0} = -(L-x),$$

$$\frac{\partial T_x}{\partial F_0} = L'.$$



(IV) Section in DB

M_o imposes a bending moment = M_o , and a torsional moment = 0.

T_o imposes a bending moment = 0, and a torsional moment = T_o .

$$M_x = M_o + 0 - F_o \cdot y + 0 = M_o - F_o y \text{ -----(j)}$$

$$T_x = 0 + T_o + 0 + 0 = T_o \text{ -----(k)}$$

which gives

$$\frac{\partial M_x}{\partial M_o} = 1,$$

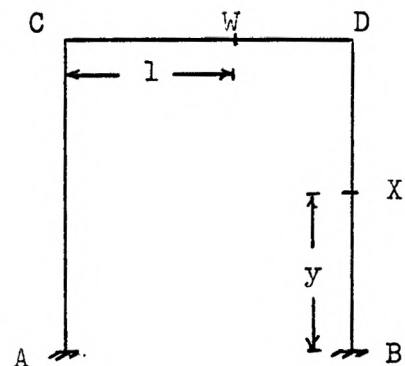
$$\frac{\partial T_x}{\partial M_o} = 0,$$

$$\frac{\partial M_x}{\partial T_o} = 0,$$

$$\frac{\partial T_x}{\partial T_o} = 1,$$

$$\frac{\partial M_x}{\partial F_o} = -y,$$

$$\frac{\partial T_x}{\partial F_o} = 0.$$



Now, using equation (a), we find

$$\begin{aligned} & \frac{1}{EI} \left[\int_0^{L'} \left\{ -M_o + F_o y + W(L' - y) \right\} (-1) dy + \int_0^{L'} \left\{ M_o - F_o y \right\} (1) dy \right] \\ & + \frac{1}{NJ} \left[\int_0^L (-M_o + F_o L') (-1) dx + \int_0^L (-M_o + F_o L') (-1) dx \right] = 0 \\ \text{or } & \frac{1}{EI} \left[\left\{ M_o L' - \frac{F_o L'^2}{2} - \frac{W L'^2}{2} \right\} + \left\{ M_o L' - \frac{F_o L'^2}{2} \right\} \right] + \frac{1}{NJ} \left[\left\{ M_o L - F_o L L' \right\} \right. \\ & \left. + \left\{ M_o (L-1) - F_o \frac{(L-1)L'}{2} \right\} \right] = 0 \end{aligned}$$

$$\text{or } \frac{1}{EI} \left[2M_o L' - F_o L'^2 - \frac{W L'^2}{2} \right] + \frac{1}{NJ} \left[M_o L - F_o L L' \right] = 0 \text{ -----(A)}$$

For the load at the middle point of CD, $l = L/2$ and $F_o = W/2$, so that

Equation (A) becomes,

$$\frac{1}{EI} \left[2M_o L' - \frac{W}{2} L'^2 - \frac{W L'^2}{2} \right] + \frac{1}{NJ} \left[M_o L - \frac{W}{2} L L' \right] = 0,$$

$$\text{or } M_o = \frac{2W L'^2 NJ + W L L' EI}{2(2L' NJ + LEI)} \text{ -----(Aa)}$$

Now, using Equation (b), we find

$$\begin{aligned} & \frac{1}{EI} \left[\int_0^L \{T_0 - F_0(L-x) + W(1-x)\} (1) dx + \int_1^L \{T_0 - F_0(L-x)\} (1) dx \right] \\ & + \frac{1}{NJ} \left[\int_0^L \{-T_0 + F_0L - W1\} (-1) dx + \int_0^L T_0 dx \right] = 0 \\ \text{or } & \frac{1}{EI} \left[T_0L - \frac{F_0L^2}{2} + \frac{WL^2}{2} \right] + \frac{1}{NJ} \left[2T_0L' - F_0LL' + WL' \right] = 0. \end{aligned} \quad \text{-----(B)}$$

For the load at the middle point of CD, $1 = L/2$ and $F_0 = W/2$, so that Equation (B) becomes

$$\begin{aligned} & \frac{1}{EI} \left[T_0L - \frac{WL^2}{8} \right] + \frac{1}{NJ} \left[2T_0L' \right] = 0 \\ \text{or } & T_0 = \frac{WL^2NJ}{8(NJL + 2EIL')} \quad \text{----- (Ba)} \end{aligned}$$

Now, using Equation (c), we obtain

$$\begin{aligned} & \frac{1}{EI} \left[\int_0^L \{-M_0 + F_0y + W(L'-y)\} y dy + \int_0^1 \{T_0 - F_0(L-x) + W(1-x)\} \{-(L-x)\} dx \right. \\ & \quad \left. + \int_1^L \{T_0 - F_0(L-x)\} \{-(L-x)\} dx + \int_0^L \{M_0 - F_0y\} (-y) dy \right] \\ & + \frac{1}{NJ} \left[\int_0^L \{-T_0 + F_0L - W1\} L dy + \int_0^1 \{-M_0 + F_0L'\} L' dx + \int_1^L \{-M_0 + F_0L'\} (L') dx \right. \\ & \quad \left. + 0 \right] = 0 \\ \text{or } & \frac{1}{EI} \left[-M_0L'^2 + \frac{2}{3} F_0L'^3 + \frac{WL'^3}{6} - T_0\frac{L^2}{2} + F_0\frac{L^3}{3} - \frac{WL^2}{2} + \frac{WL^3}{6} \right] \\ & + \frac{1}{NJ} \left[-T_0LL' - M_0LL' + F_0L^2L' + F_0L'^2L - WLL' \right] = 0 \end{aligned} \quad \text{----- (C)}$$

Load in AC

(I) Section in AC

(a) Section in AW

$$M_X = -M_O + F_O y + W(1-y)$$

$$T_X = -T_O + F_O L$$

which gives,

$$\frac{\partial M_X}{\partial M_O} = -1,$$

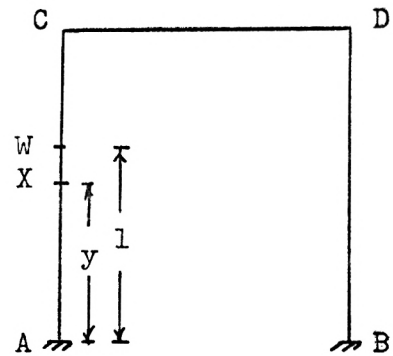
$$\frac{\partial T_X}{\partial M_O} = 0,$$

$$\frac{\partial M_X}{\partial T_O} = 0,$$

$$\frac{\partial T_X}{\partial T_O} = -1,$$

$$\frac{\partial M_X}{\partial F_O} = y,$$

$$\frac{\partial T_X}{\partial F_O} = L.$$



(b) Section in WC

$$M_X = -M_O + F_O y,$$

$$T_X = -T_O + F_O L,$$

which gives

$$\frac{\partial M_X}{\partial M_O} = -1,$$

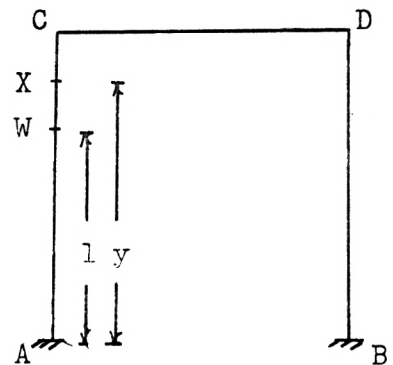
$$\frac{\partial T_X}{\partial M_O} = 0,$$

$$\frac{\partial M_X}{\partial T_O} = 0,$$

$$\frac{\partial T_X}{\partial T_O} = -1,$$

$$\frac{\partial M_X}{\partial F_O} = y,$$

$$\frac{\partial T_X}{\partial F_O} = L.$$



(II) Section in CD

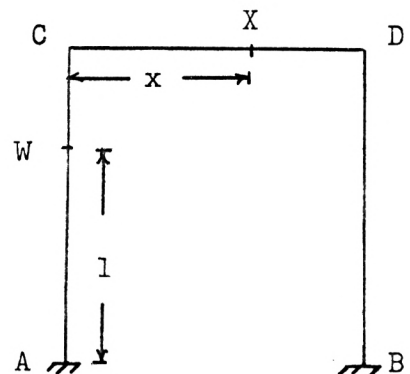
$$M_X = T_O - F_O(L-x)$$

$$T_X = -M_O + F_O L',$$

which gives

$$\frac{\partial M_X}{\partial M_O} = 0,$$

$$\frac{\partial T_X}{\partial M_O} = -1,$$



$$\frac{\partial M_x}{\partial T_o} = 1,$$

$$\frac{\partial T_x}{\partial T_o} = 0,$$

$$\frac{\partial M_x}{\partial F_o} = -(L-x),$$

$$\frac{\partial T_x}{\partial F_o} = L'.$$

(III) Section in DB

$$M_x = M_o - F_o y,$$

$$T_x = T_o,$$

which gives

$$\frac{\partial M_x}{\partial M_o} = 1,$$

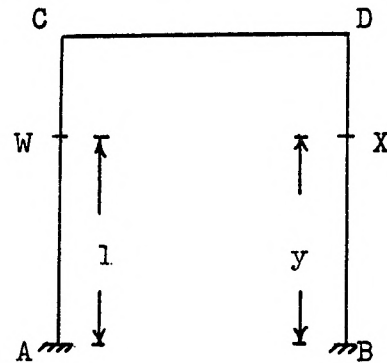
$$\frac{\partial T_x}{\partial M_o} = 0,$$

$$\frac{\partial M_x}{\partial T_o} = 0,$$

$$\frac{\partial T_x}{\partial T_o} = 1,$$

$$\frac{\partial M_x}{\partial F_o} = -y,$$

$$\frac{\partial T_x}{\partial F_o} = 0.$$



Therefore, using Equation (a), we obtain

$$\begin{aligned} & \frac{1}{EI} \left[\int_0^L \{-M_o + F_o y + W(1-y)\} (-1) dy + \int_0^L \{-M_o + F_o y\} (-1) dy + 0 + \int_0^L (M_o - F_o y) \cdot 1 \cdot dy \right] \\ & + \frac{1}{NJ} \left[\int_0^L (-M_o + F_o L') (-1) dx \right] = 0 \\ \text{or } & \frac{1}{EI} \left[2M_o L' - F_o L'^2 - \frac{WL^2}{2} \right] + \frac{1}{NJ} [M_o L - F_o LL'] = 0 \quad \text{----- (D)} \end{aligned}$$

Now, using Equation (b), we obtain

$$\begin{aligned} & \frac{1}{EI} \left[\int_0^L \{T_o - F_o(L-x)\} (1) dx \right] + \frac{1}{NJ} \left[\int_0^L (-T_o + F_o(L)) (-1) dy + \int_0^L T_o (1) dy \right] = 0 \\ \text{or } & \frac{1}{EI} \left[T_o L - \frac{F_o L^2}{2} \right] + \frac{1}{NJ} [2T_o L' - F_o LL'] = 0 \quad \text{----- (E)} \end{aligned}$$

Now, using Equation (c), we find

$$\begin{aligned} \frac{1}{EI} \left[\int_0^L \{-M_0 + F_0 y + W(1-y)\} y dy + \int_1^{L'} \{-M_0 + F_0 y\} y dy \right. \\ \left. + \int_0^L \{T_0 - F_0(L-x)\} \{- (L-x)\} dx + \int_0^L (M_0 - F_0 y) (-y) dy \right] \\ + \frac{1}{NJ} \left[\int_0^L (-T_0 + F_0 L) L dy + \int_1^{L'} (-T_0 + F_0 L) L dy + \int_0^L (-M_0 + F_0 L') L' dx \right] = 0 \end{aligned}$$

which gives

$$\begin{aligned} \frac{1}{EI} \left[-M_0 L'^2 + \frac{2}{3} F_0 L'^3 + \frac{F_0 L^3}{3} - \frac{T_0 L^2}{3} + \frac{WL^3}{6} \right] \\ + \frac{1}{NJ} \left[-T_0 LL' + F_0 L^2 L' + F_0 L'^2 L - M_0 LL' \right] = 0 \text{ ----- (F)} \end{aligned}$$

Load in BD

Since the model is symmetrical, the above equations for the load in AC can be used for the determination of bending moment, torsional moment and shear force at any point along the center line of the model for the load in DB.

The equations so derived were used for the actual analysis of the frame models. Sample calculations are given below for model no. 1, with the 1 lb. load at Sta. 5. All of the rest of the calculations for other load positions and models were done in a similar fashion and are shown in a tabular form at the end of this chapter.

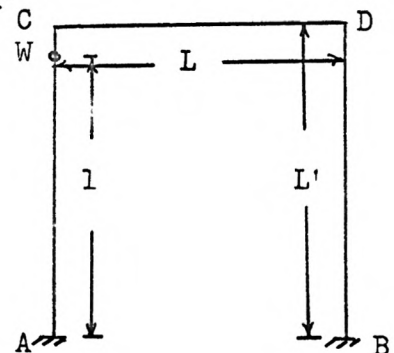
Sample Calculations for Model No. 1, Load at Sta. 5.

Here, $L = 5.525''$

$L' = 8.5''$

$l = 7.5''$

$W = 1 \text{ lb.}$



Also, we know that $EI = 430,000 \times 0.0011 = 473 \text{ Lbs.-in}^2$

and $GJ = 171,000 \times 0.00352 = 601 \text{ Lbs.-in}^2$.

Therefore, using equation (D), with the above values, we obtain

$$\frac{1}{473} \left[2M_0 \times 8.5 - F_0 \times (8.5)^2 - \frac{1 \times (7.5)^2}{2} \right] + \frac{1}{601} \left[M_0 \times 5.525 - F_0 \times 8.5 \right. \\ \left. \times 5.525 \right] = 0$$

$$\text{or } M_0 = 5.12F_0 + 1.319 \text{ -----(i)}$$

Using Equation (E), we obtain

$$\frac{1}{473} \left[5.525T_0 - 15.25F_0 \right] + \frac{1}{601} \left[17T_0 - 47F_0 \right] = 0 \text{ or } T_0 = 2.76F_0 \text{ ---(ii)}$$

Using Equation (F), we obtain

$$\frac{1}{473} \left[-M_0 \times (8.5)^2 + \frac{2}{3} F_0 \times (8.5)^3 + \frac{1}{3} F_0 \times (5.525)^3 - T_0 \times \frac{(5.525)^2}{2} + \frac{1}{6} \times (7.5)^3 \right] \\ + \frac{1}{601} \left[-(8.5) \times (5.525) T_0 + (8.5)(5.525)^2 F_0 + F_0 (8.5)^2 (5.525) \right. \\ \left. - M_0 (8.5)(5.525) \right] = 0$$

$$\text{or } -139M_0 + 1251.3F_0 - 66.4T_0 + 89.5 = 0 \text{ -----(iii)}$$

Now, substituting the values of M_0 , and T_0 from Equations (i) and (ii) above into Equation (iii), we find

$$-139(5.12F_0 + 1.319) + 1251.3F_0 - 66.4(2.76F_0) + 89.5 = 0,$$

which gives

$$F_0 = 0.263 \text{ Lbs.}$$

From (i), and (ii), we obtain

$$M_0 = 2.667 \text{ Lbs. In. and } T_0 = 0.726 \text{ Lbs. In.}$$

So, we now know the redundants and can, therefore, determine the moments and torsions at all points along the centerline of the model by using Equations (d) to (k).

Section in AC

(I) Section in AW

The bending and torsional moments for a section in AW are calculated as follows:

At a point 0" from the fixed end A(i.e. at $y = 0$ or at A),

$$\begin{aligned} M_y &= -M_0 + F_0 y + W(1-y) = -2.667 + 0.263 \times 0 + 1(7.5-0) \\ &= +\underline{4.833} \text{ In. Lbs.} \end{aligned}$$

$$\text{and } T_y = -T_0 + F_0 L = -0.726 + 0.263 \times 5.525$$

$$= +\underline{0.726} \text{ In. Lbs.}$$

$$\text{At a point 1" from A, } M_y = -2.667 + 0.263 \times 1 + 1.(7.5-1) = \underline{4.096} \text{ In. Lbs.}$$

$$\text{and } T_y = -0.726 + 0.263 \times 5.525 = +\underline{0.726} \text{ In. Lbs.}$$

Similarly, other values, at one inch intervals, were calculated and are given in a tabular form below:

TABLE NO. 5

y in inches	M_y in In. Lbs.	T_y in In. Lbs.
2"	+3.359	+0.726
3"	+2.662	+0.726
4"	+1.885	+0.726
5"	+1.148	+0.726
6"	+0.411	+0.726
7"	-0.326	+0.726

(II) Section in WC

At a point 8" from A, (i.e at $y = 8"$)

$$M_y = -M_o + F_o y = -2.667 + 0.263 \times 8 = \underline{-0.563} \text{ Inch Lbs.}$$

$$T_y = -T_o + F_o L = -0.726 + 0.263 \times 5.525 = \underline{+0.726} \text{ Inch Lbs.}$$

At a point 8.5" from A,

$$M_y = -M_o + F_o y = -2.667 + 0.263 \times 8.5 = \underline{-0.563} \text{ Inch Lbs.}$$

$$\text{and } T_y = -T_o + F_o L = \underline{0.726} \text{ Inch Lbs.}$$

Section in CD

At C, (or at $x = 0"$),

$$M_x = T_o - F_o (L-x) = 0.726 - 0.263 (5.525 - 0) = \underline{-0.726} \text{ Inch Lbs.}$$

$$\text{and } T_x = -M_o + F_o L' = -2.667 + 0.263 \times 8.5 = \underline{-0.430} \text{ Inch Lbs.}$$

Similarly other values were calculated and are given in a tabular form below:

TABLE NO. 6

x in inches	M _x in Inch Lbs.	T _x in Inch Lbs.
1"	-0.464	-0.430
2"	-0.202	-0.430
3"	+0.061	-0.430
4"	+0.325	-0.430
5"	+0.588	-0.430
5.525"	+0.726	-0.430

Section in DB

At B, (i.e. $y = 0$ "),

$$M_y = M_o - F_o y = 2.667 - 0.263 \times 0 = \underline{+2.667} \text{ Inch Lbs.}$$

and $T_y = T_o = +0.726 \text{ In. Lbs.}$

Similarly other values were calculated and are given in a tabular form below:

TABLE NO. 7

y in inches	M _y in Inch Lbs.	T _y in Inch Lbs.
1	+2.404	+0.726
2	+2.141	+0.726
3	+1.878	+0.726
4	+1.615	+0.726
5	+1.352	+0.726
6	+1.089	+0.726
7	+0.826	+0.726
8	+0.563	+0.726
9	+0.430	+0.726

All the other results for other loads positions were obtained in a similar way and are shown in the following tables. The theoretical Bending Moment, Shear Force and Torsional Moment diagrams are shown in Figs. 23 - 30.

Theoretical Results

Model No. 1

(Load = 1 Lb., E = 425ksi)

TABLE NO. 8

Load at sta.	F_o in Lbs.	M_o in Inch Lbs.	T_o in Inch Lbs.
1	--	--	--
2	0.0654	0.551	0.183
3	0.1296	1.138	0.358
4	0.201	1.876	0.555
5	0.263	2.667	0.726
6	0.285	3.150	0.787
7	0.393	3.705	0.545
8	0.50	4.26	0.215
9	0.600	4.795	-0.244
10	0.713	5.35	-0.787
11	0.746	4.883	-0.726
12	0.824	4.124	-0.555
13	0.905	3.362	-0.358
14	0.942	2.449	-0.183
15	--	--	--

Theoretical Results

Model No. 2

(Load = 1.48 Lbs., E = 430ksi)

TABLE NO. 9

Load at sta.	F ₀ in Lbs.	M ₀ in Inch Lbs.	T ₀ in Inch Lbs.
1	--	--	--
2	0.0643	0.4207	0.1775
3	0.127	0.882	0.351
4	0.1965	1.464	0.542
5	0.261	2.124	0.721
6	0.290	2.50	0.801
7	0.488	3.19	0.623
8	0.740	4.082	0.393
9	0.998	4.98	0.028
10	1.176	5.64	-0.801
11	1.226	--	-0.721
12	1.272	4.456	-0.543
13	1.368	3.558	-0.350
14	1.410	2.539	-0.1775
15	--	--	--

Theoretical Results

Model No. 3

(Load = 1.48 Lbs., E = 430ksi)

TABLE NO. 10

Load at sta.	F_o in Lbs.	M_o in Inch Lbs.	T_o in Inch Lbs.
1	--	--	--
2	0.0995	0.436	0.201
3	0.1350	0.910	0.370
4	0.163	1.208	0.451
5	0.424	1.848	0.540
6	0.74	2.61	0.509
7	1.022	3.381	0.248
8	1.435	4.31	-0.449
9	1.332	3.532	-0.370
10	2.08	3.94	-0.201
11	--	--	--

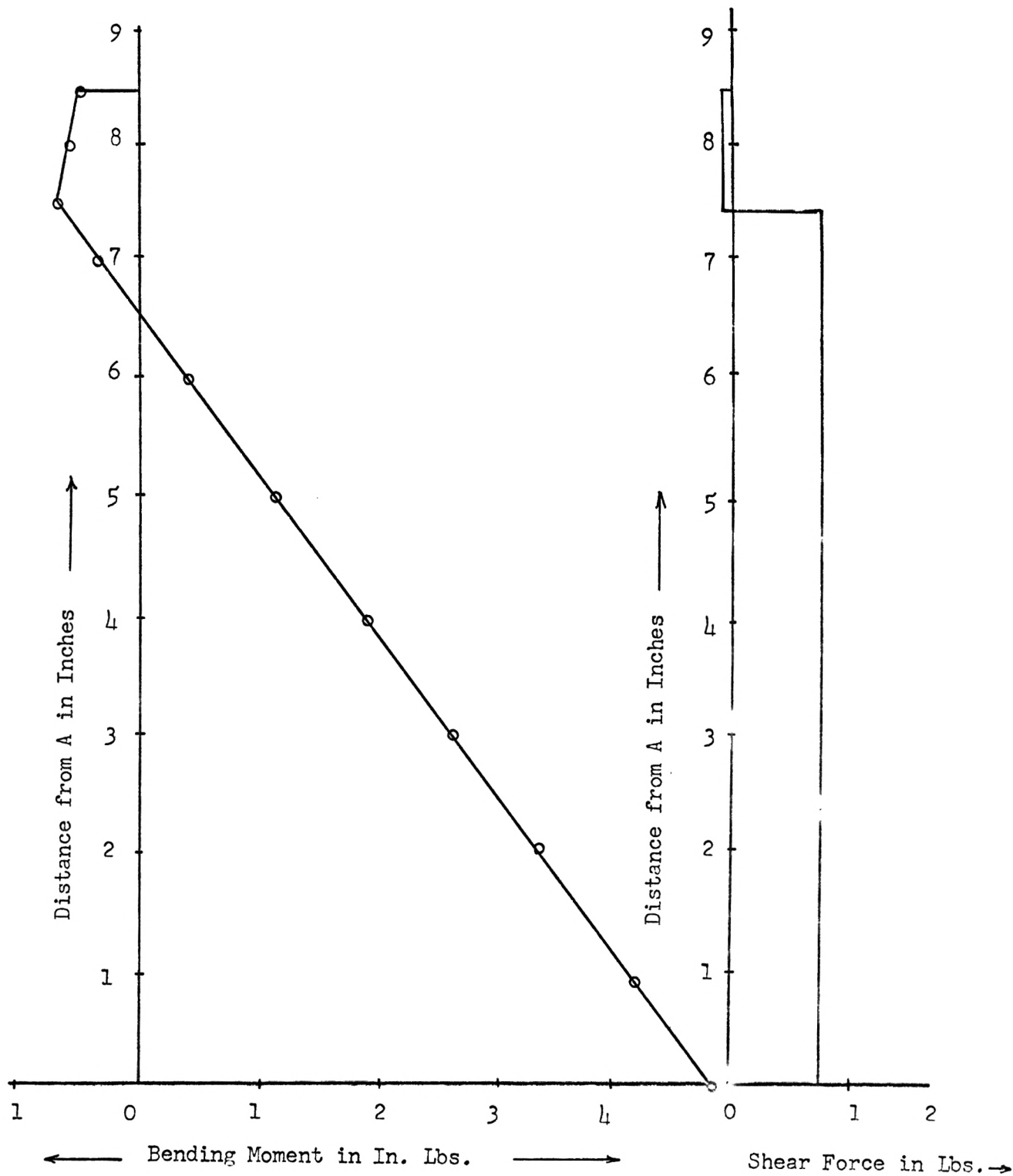


Fig. 23

Fig. 24

Theoretical Bending Moment and Shear Force diagrams for the leg AC with load
at sta. 5

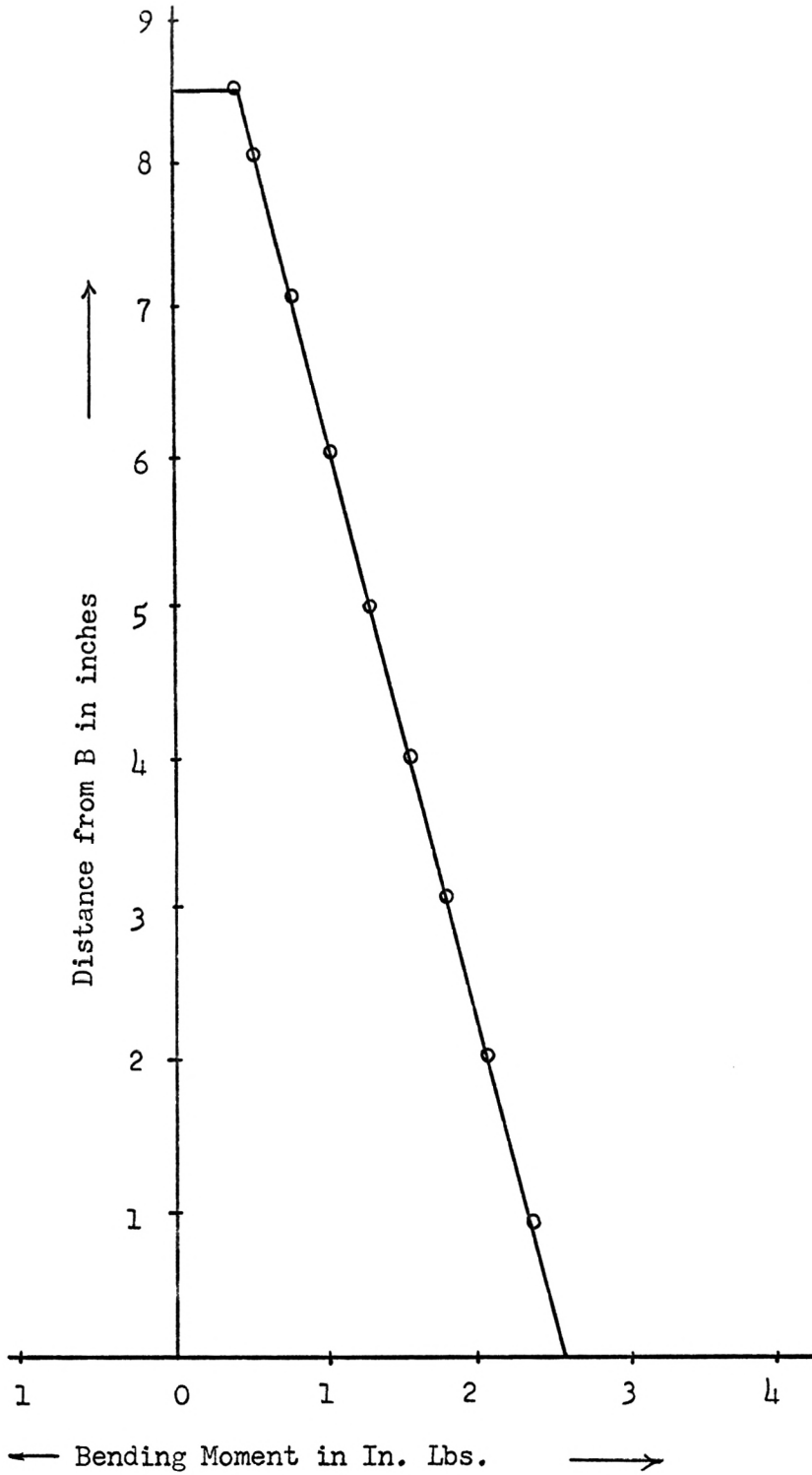


Fig. 25

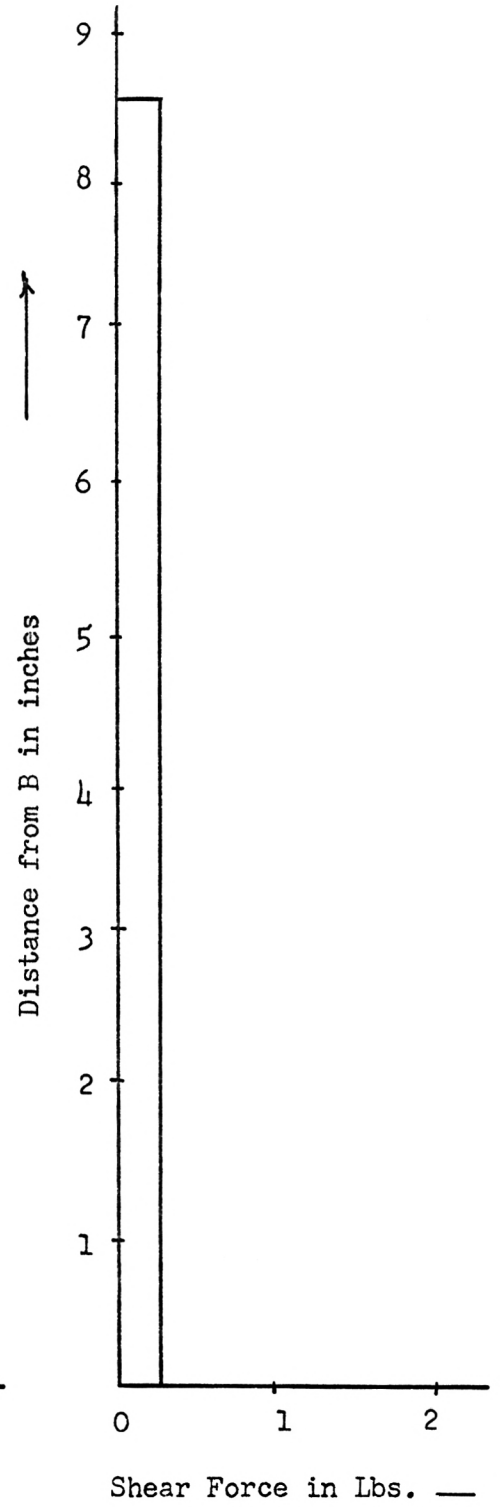


Fig. 26

Theoretical Bending Moment and Shear Force diagrams for leg BD with load at
sta. 5

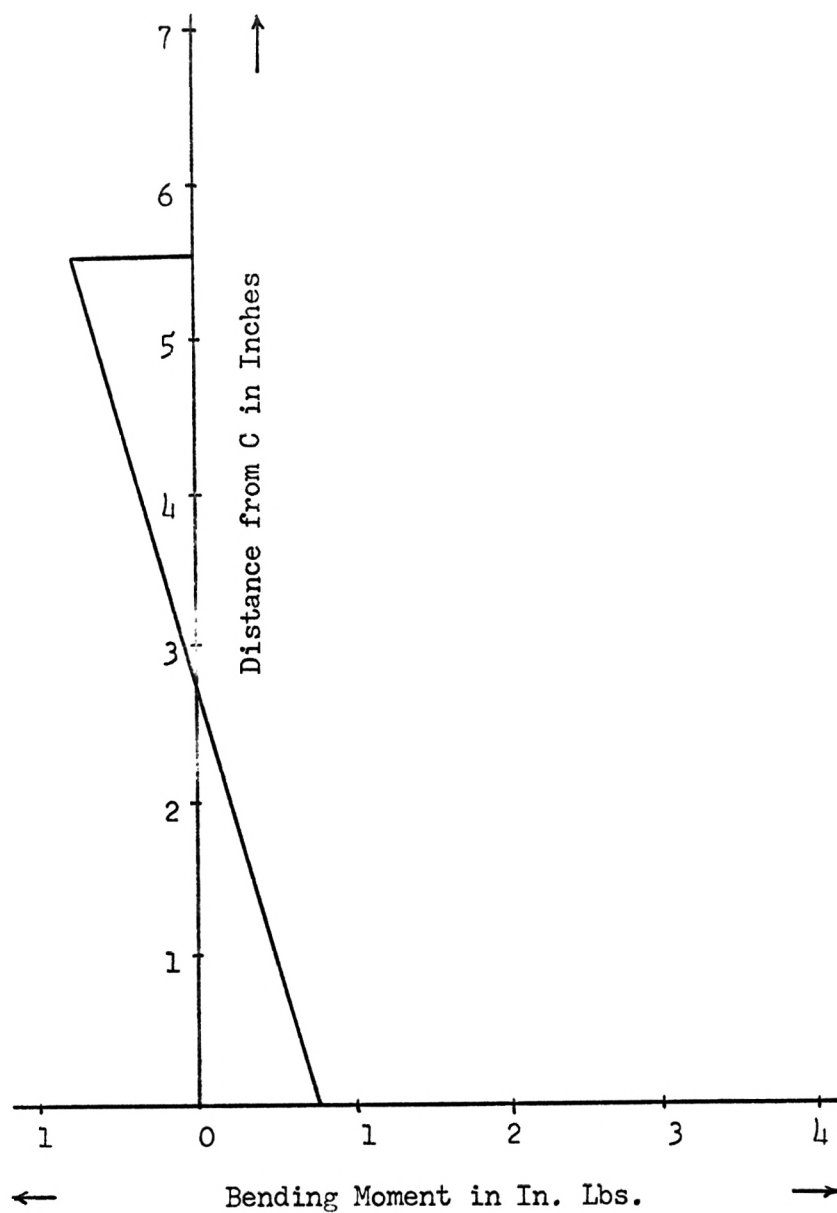


Fig. 27

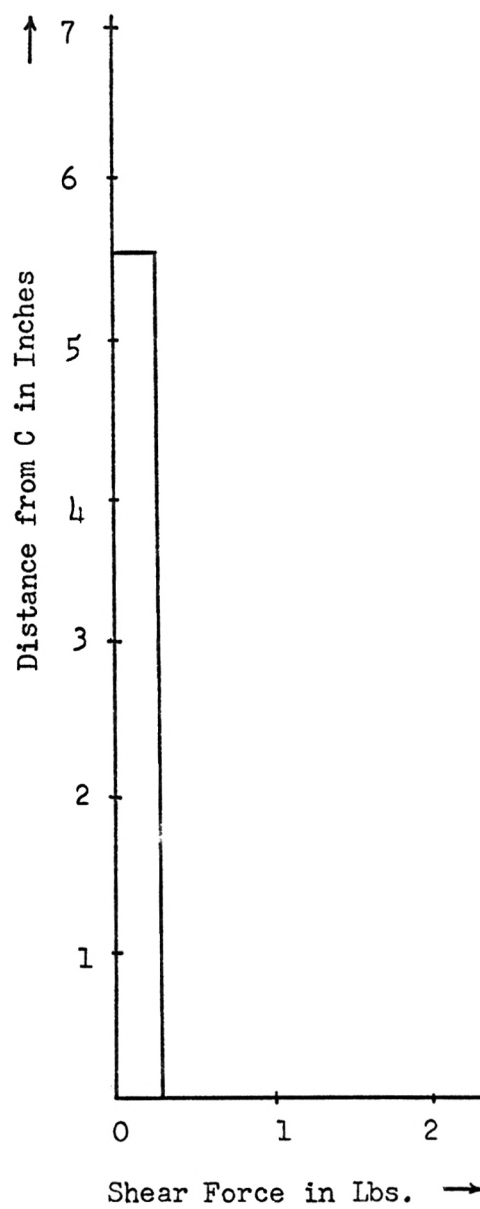
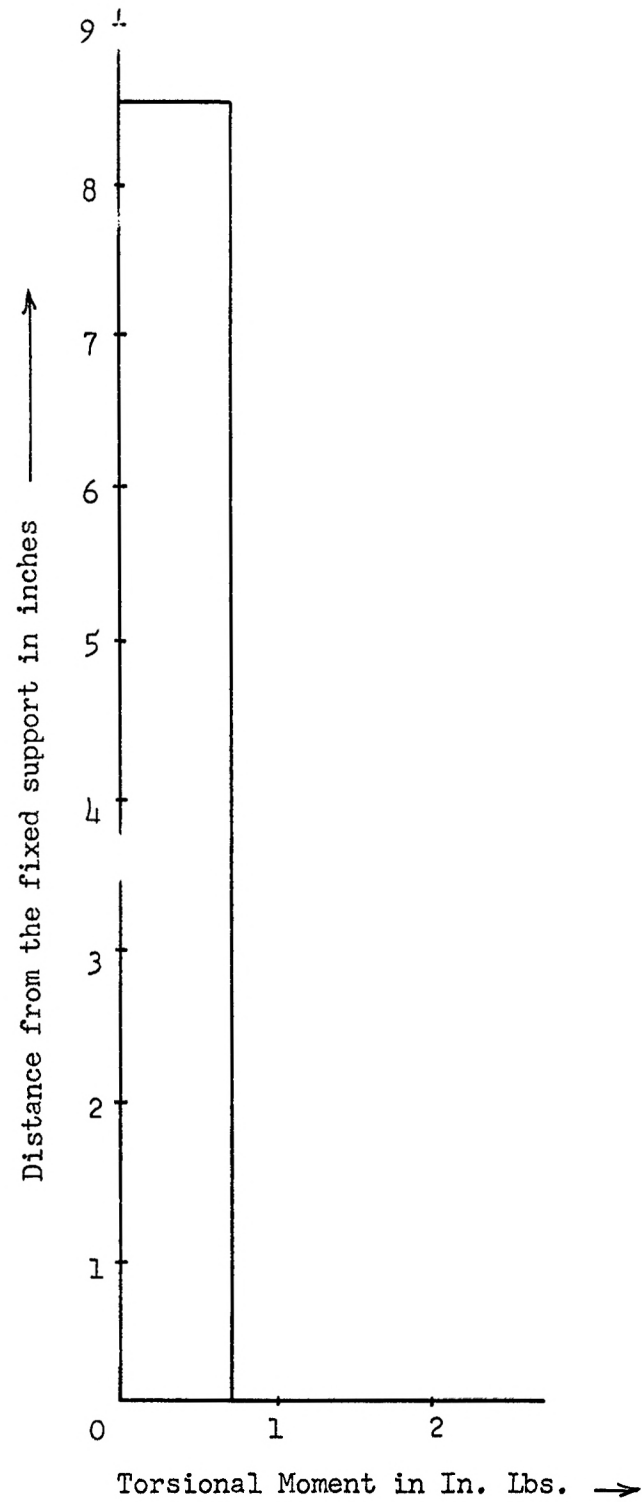


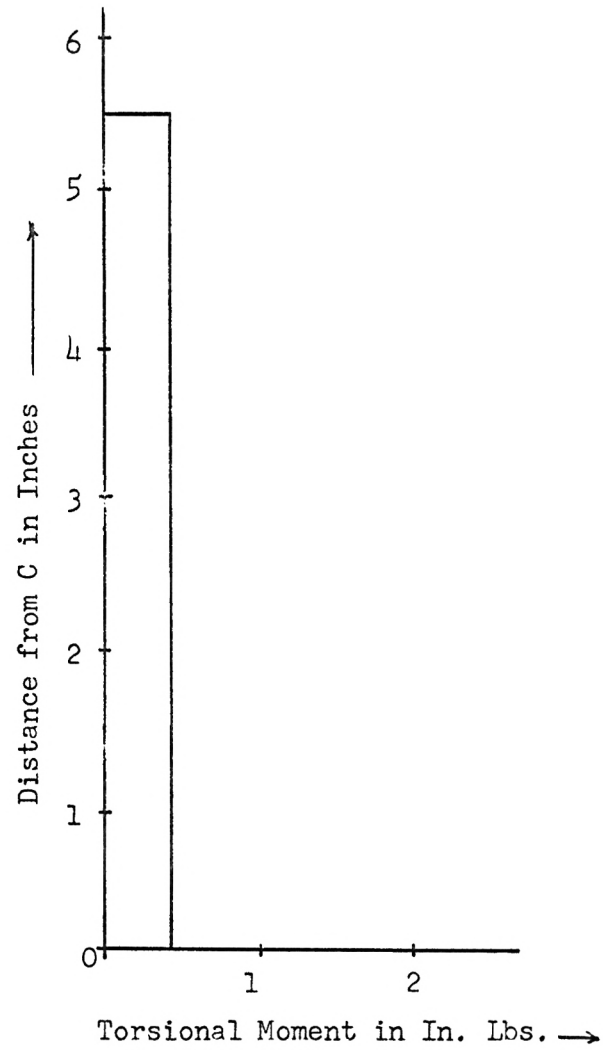
Fig. 28

Theoretical Bending Moment and Shear Force diagrams for beam
CD with load at sta. 5



Theoretical Torsional Moment diagram for leg AC or BD with load at sta. 5

Fig. 29



Theoretical Torsional Moment diagram for beam CD with
load at sta. 5

Fig. 30

COMPARISON AND DISCUSSION OF RESULTS

Tables (11), (12) and (13) show the final experimental and theoretical results along with the percentage errors for models nos. (1), (2) and (3), for the bending moments, torsional moments and the shearing forces at the fixed end B, which were taken as redundants in the analysis. The experimental results were found to be in good agreement with the theoretical results. The percentage error varied from a minimum of zero percent to a maximum of 19%, with an average value of approximately 6 to 7%.

There were probably several sources of error. First, a slight error in the measurement of fringe spacings would result in a magnified error in the final results. As has already been mentioned, some of the photographs had dim fringes on one of the legs which made it difficult to measure their spacings very accurately. The dim fringes on one of the legs of those photographs might have been due to the model surface not being exactly parallel to the camera front, making the distance to that leg from the camera lens larger or smaller than that of the other leg. The accuracy of results also depends on the accurate plotting of the fringe order versus distance curves. The bending moment and torsional moment diagrams are plotted with the aid of the values of Δy obtained from these curves and a slight error in the values of Δy affects the values of bending and torsional moments quite considerably.

Also, at the built-in supports, the last interference fringe is always at a very little distance from the support. Thus for the fringe order versus distance curve, a little extrapolation is necessary, resulting sometimes in reduced accuracy. The accuracy is also reduced very near the

concentrated load, in part because of the fact that the theory is applicable to the middle plane of the model, whereas measurements are taken from the surface. Further, near a concentrated load, the stresses normal to the plane of the model are not close to zero even though they are assumed to be.

Other comparatively insignificant sources of error may include the presence of a few small unseen wrinkles on the grid paper due to changes in temperature or humidity. In some cases, the full applied load might not have been transferred to the model because of a little friction in the lever bearing and because of the load arm not being exactly perpendicular to the model surface. Taking into consideration all these sources of error, an accuracy of 6-7% was considered to be quite satisfactory.

The behaviour of the frame models under a moving load and the deviation of the experimental results from the theoretical results can be understood more easily from the influence line diagrams for M_o , F_o and T_o , shown in Figs. (31) through (39). It will be noticed that as the load moves from A to C, the values of bending moment, torsional moment and shearing force increase parabolically. Then, as the load moves from C to D, the bending moment and shearing force increase by a straight line relationship, while the torsional moment decreases parabolically, becoming zero at some point between the middle point of CD and the corner D, changes sign and then continues to vary parabolically till it reaches a maximum negative value as the load reaches D. As the load moves further from D to B, the bending and torsional moments, with opposite signs, decrease parabolically to a zero value at B, but the shearing force goes on increasing, becoming a maximum when the load reaches B. The shearing force, therefore, does not change sign as the load moves from A to B. The bending moment also does not change

sign and is maximum when the load is at D. But, the torsional moment changes sign. Thus the maximum positive value of torsional moment occurs when the load is at C and the maximum negative value occurs when the load is at D.

As far as the general behaviour of the three models is concerned, it is quite clear from the influence-line diagrams that it is almost the same for the three of them. The change in the width-height ratio, therefore, does not have much effect, with the exception that as the height is increased with respect to the width, the point of contra-flexure in the torsional moment diagram shifts away from the corner D.

Comparison of Experimental and Theoretical Results

MODEL NO. 1 (Load = 1 Lb., E = 425 ksi)

TABLE NO. 11

Load at sta.	F _o in Lbs.			M _o in inch Lbs.			T _o in inch Lbs.		
	Theoretical	Experimental	% age error	Theoretical	Experimental	% age error	Theoretical	Experimental	% age error
1	--	--	--	--	--	--	--	--	--
2	0.0650	--	--	0.551	0.545	-1.09	0.183	--	--
3	0.1335	0.1265	+5.25	0.138	1.050	-7.74	0.358	0.386	+7.83
4	0.201	0.1706	-14.80	1.876	1.50	-19.9	0.555	0.535	-3.60
5	0.263	0.244	-6.46	2.667	2.40	-9.90	0.726	0.771	+6.20
6	0.285	0.246	-14.00	3.15	2.69	-14.6	0.787	0.803	+2.03
7	0.393	0.400	+1.78	3.705	3.50	-5.5	0.545	0.450	-17.40
8	0.50	0.492	-1.60	4.26	4.18	-1.88	0.215	--	--
9	0.60	0.600	0.00	4.795	4.68	-2.40	-0.244	--	--
10	0.713	0.687	-3.65	5.350	5.23	-2.24	-0.787	-0.803	+2.03
11	0.746	0.682	-8.56	4.883	4.50	-7.85	-0.726	-0.771	+6.20
12	0.824	0.702	-14.70	4.124	3.30	-19.99	-0.555	-0.551	-3.60
13	0.880	--	--	3.362	--	--	-0.358	-0.386	+7.83
14	0.942	0.903	-4.15	2.449	2.35	-4.06	-0.183	--	--
15	--	--	--	--	--	--	--	--	--
Average error = 6.81%			Average error = 6.26%			Average error = 6.3%			

Comparison of Experimental and Theoretical Results

MODEL NO. 2 (Load = 1 Lb., E = 430 ksi)

TABLE NO. 12

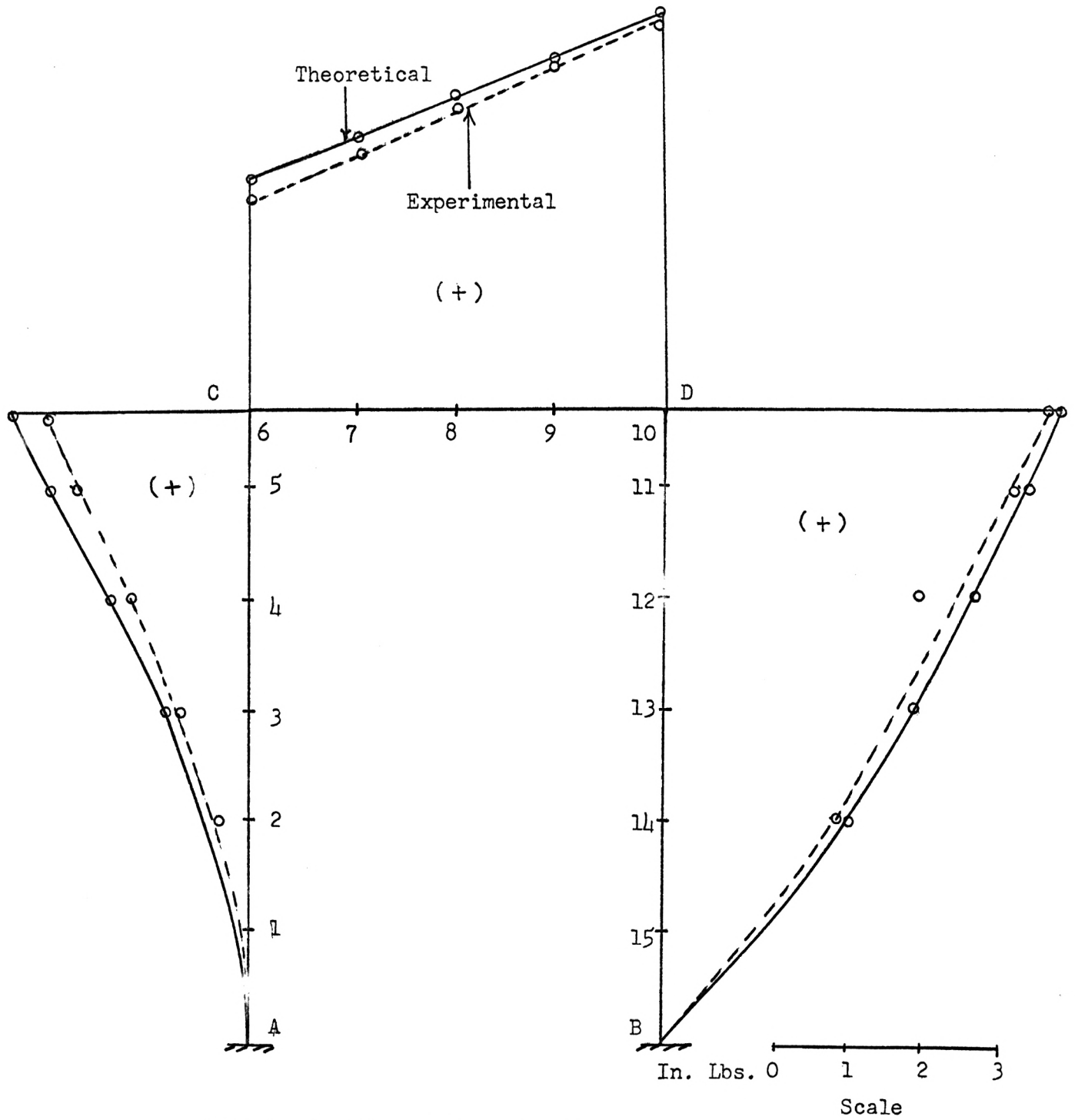
Load at sta. no.	F _o in Lbs.			M _o in Inch Lbs.			T _o in Inch Lbs.		
	Theoretical	Experimental	% age error	Theoretical	Experimental	% age error	Theoretical	Experimental	% age error
1	--	--	--	--	--	--	--	--	--
2	0.0441	--	--	0.2845	--	--	0.120	--	--
3	0.0807	--	--	0.5960	--	--	0.2569	0.276	+7.10
4	0.1328	0.1155	-13.04	0.989	0.886	-10.41	0.367	0.404	+10.10
5	0.1761	0.1850	-5.05	1.437	1.385	-3.61	0.488	--	--
6	0.1960	0.1860	-5.10	1.689	1.550	-7.94	0.541	0.556	2.79
7	0.330	0.306	-7.29	2.159	1.950	-9.71	0.421	0.414	-1.67
8	0.50	0.466	-6.80	2.760	2.570	-6.68	0.268	0.301	+12.31
9	0.672	0.646	-3.87	3.361	3.10	-7.76	0.018	--	--
10	0.792	0.706	+10.81	3.810	3.250	-14.7	-0.541	-0.556	+2.77
11	0.829	--	--	3.561	3.340	-6.2	-0.488	-0.488	0
12	0.860	0.839	-2.44	3.010	2.830	-5.99	-0.367	-0.404	+10.1
13	0.923	0.962	+4.23	2.40	2.310	-3.75	-0.2369	-0.276	+16.46
14	0.953	--	--	1.71	--	--	--	--	--
15	--	--	--	--	--	--	--	--	--
Average error = 6.52%			Average error = 7.678%			Average error = 7.07%			

Comparison of Experimental and Theoretical Results

MODEL NO. 3 (Load = 1 Lb., E = 430 ksi)

TABLE NO. 13

Load at sta.	F _o in Lbs.			M _o in Inch Lbs.			T _o in Inch Lbs.		
	Theoretical	Experimental	% age error	Theoretical	Experimental	% age error	Theoretical	Experimental	% age error
1	--	--	--	--	--	--	--	--	--
2	0.0493	0.0426	-1.36	0.295	0.255	-1.35	0.14	0.140	0
3	0.0906	0.0992	+9.50	0.615	0.551	-10.40	0.250	0.227	-9.2
4	0.1109	0.1007	-9.21	0.816	0.744	-8.83	0.3042	0.290	-4.66
5	0.2869	0.271	-5.58	1.249	1.15	-7.94	0.365	0.311	-14.88
6	0.500	0.464	-7.20	1.764	1.622	-8.05	0.344	0.395	+14.82
7	0.694	0.656	-5.48	2.285	2.096	-8.26	0.168	--	--
8	0.970	1.191	+14.34	2.910	2.739	-5.84	-0.3039	-0.290	-4.6
9	0.919	0.870	-5.23	2.385	2.178	-8.67	-0.250	-0.227	-9.2
10	--	--	--	2.660	--	--	-0.140	-0.140	0
11	1.00	--	--	--	--	--	--	--	--
Average error = 7.24%			Average error = 7.42%			Average error = 7.16%			



Unit load influence line for M_0
(Model No. 1)

Fig. 31

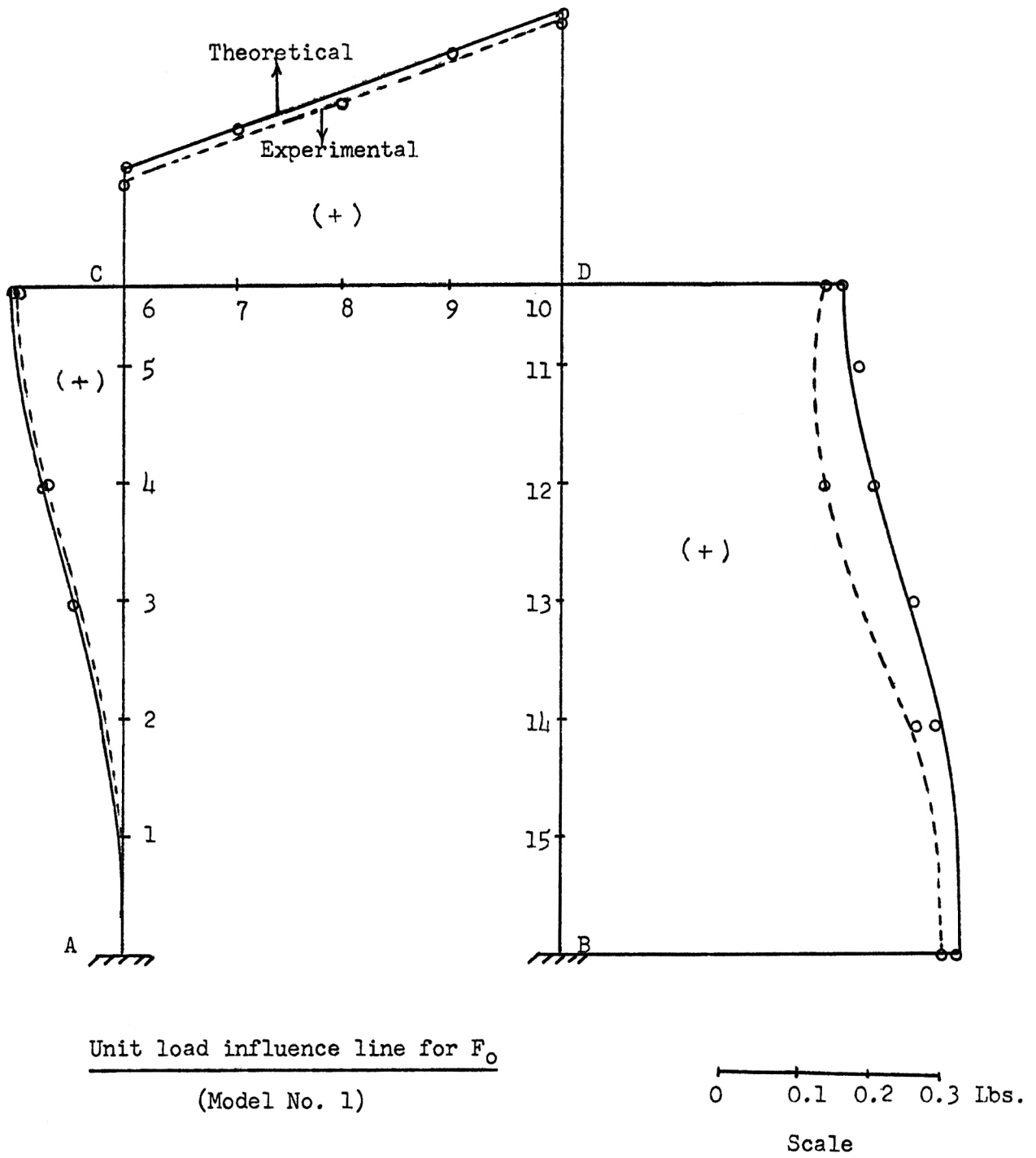


Fig. 32

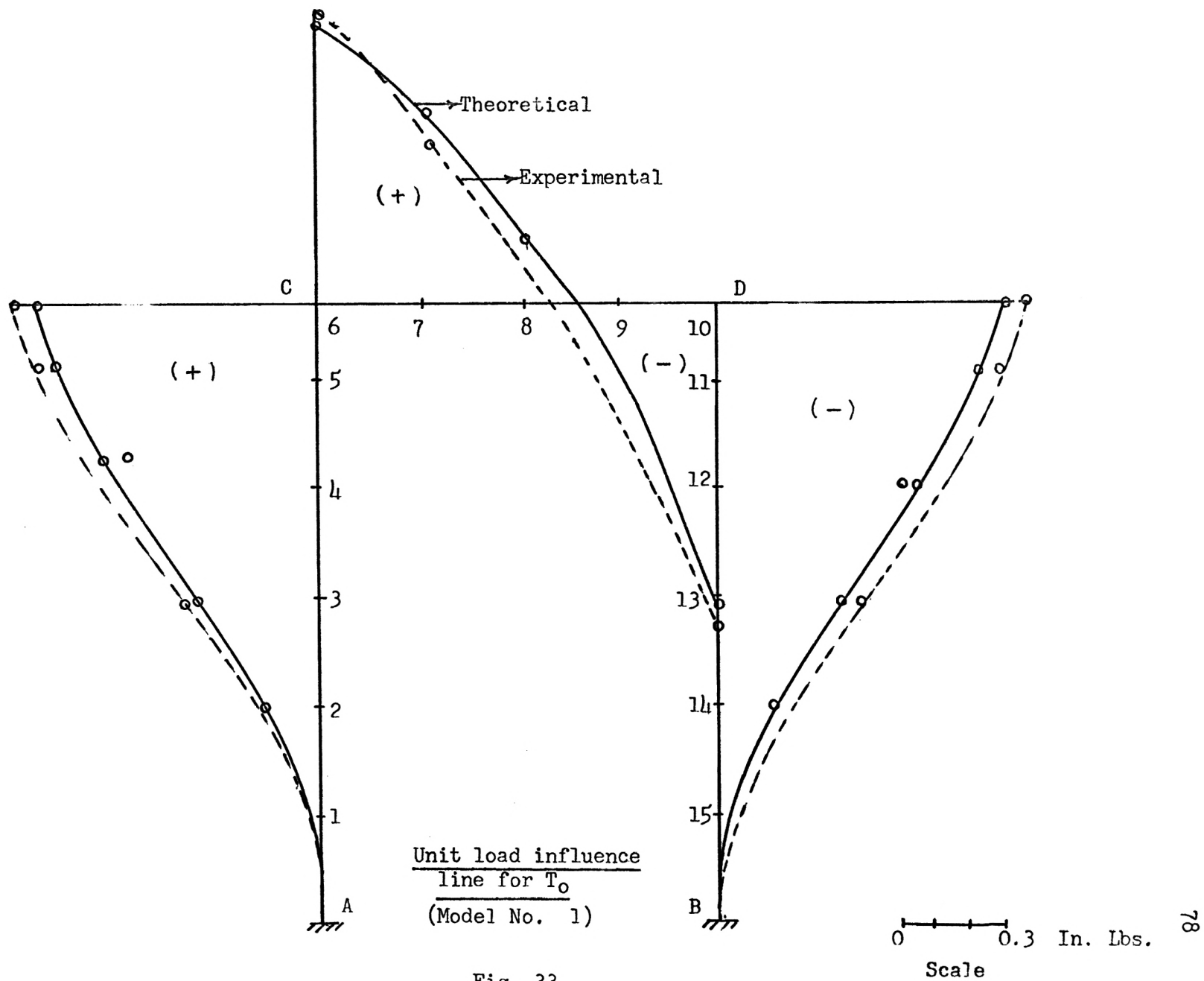
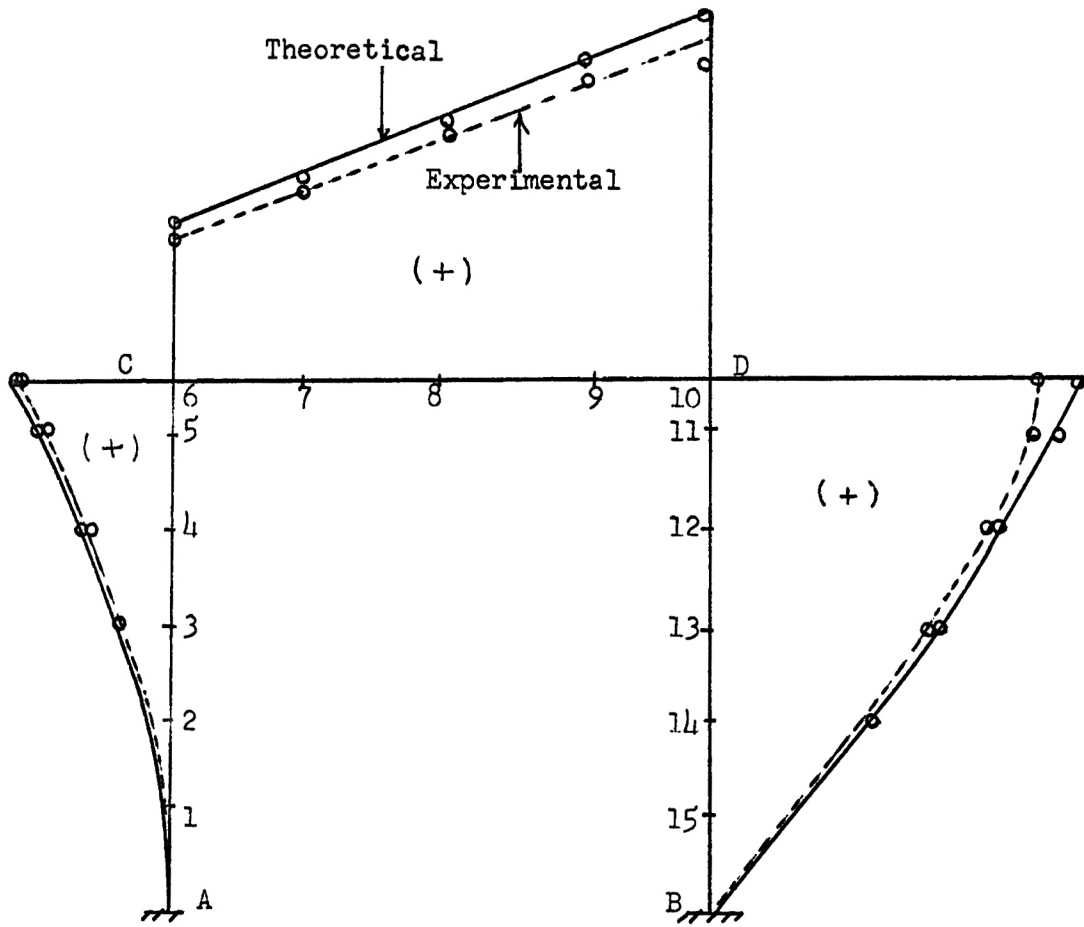


Fig. 33

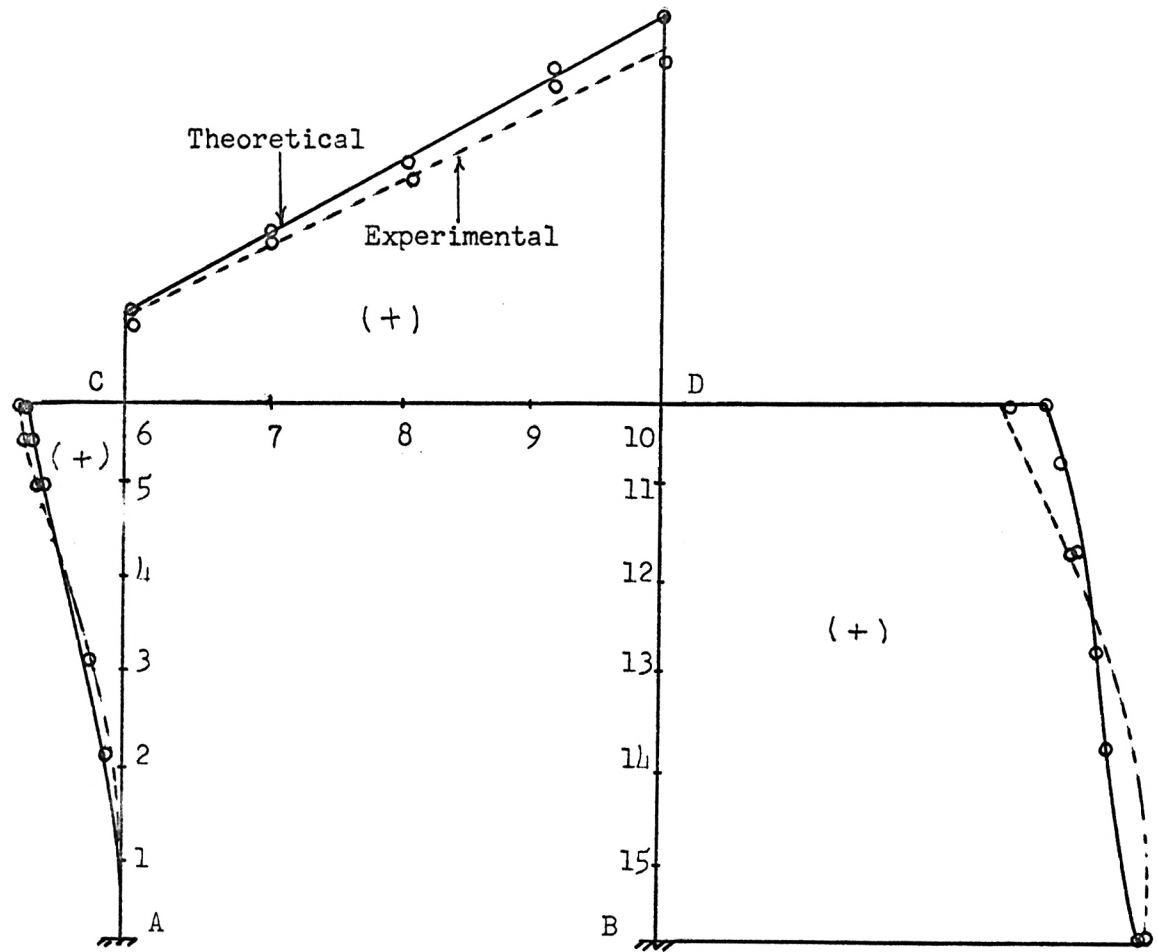


Unit load influence line for M_0

(Model No. 2)

Fig. 34

0 1 2 3 In. Lbs.
Scale



Unit load influence line for F_0

(Model No. 2)

Fig. 35

0 ——— 0.3 Lbs.

Scale

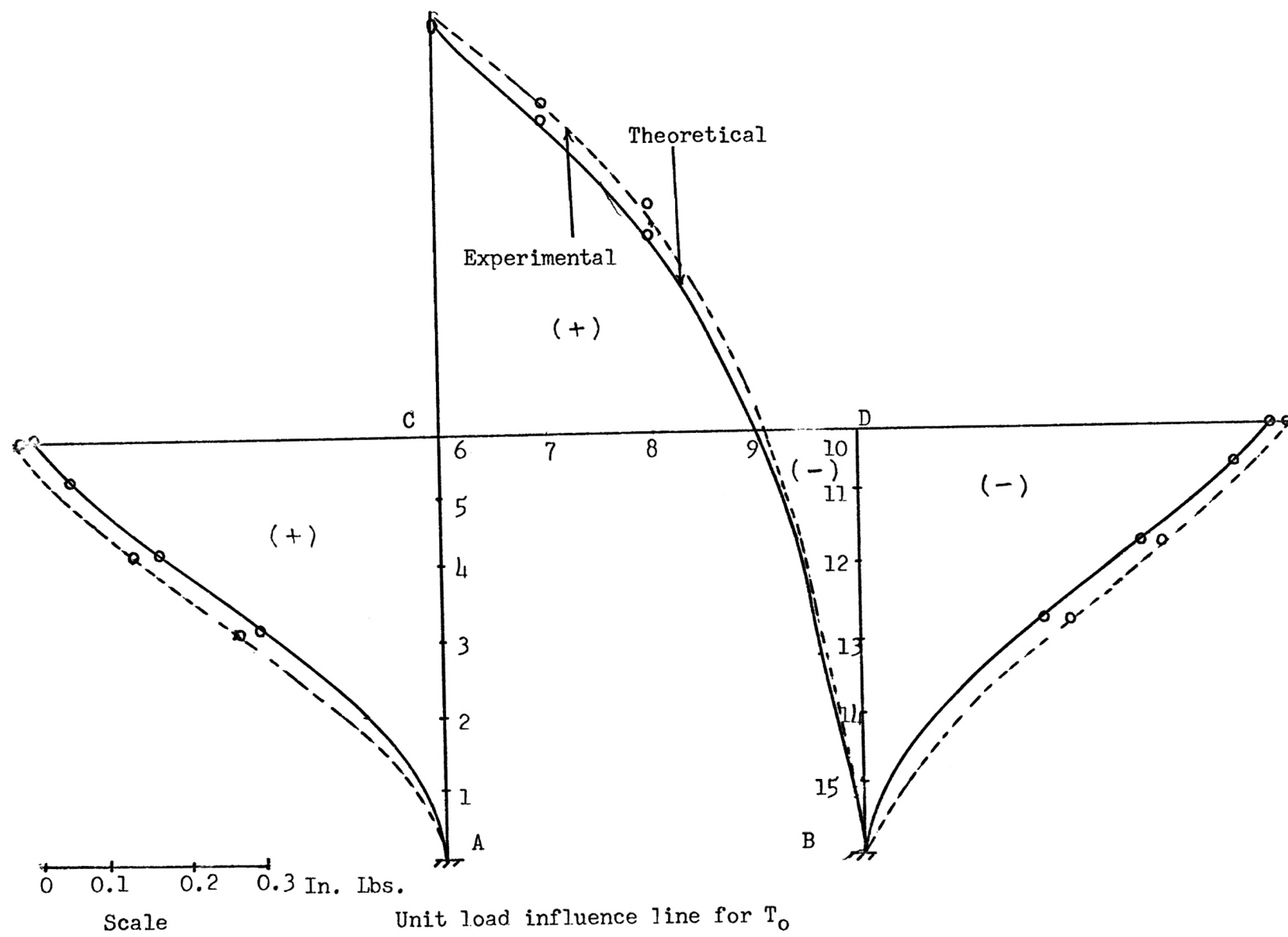


Fig. 36

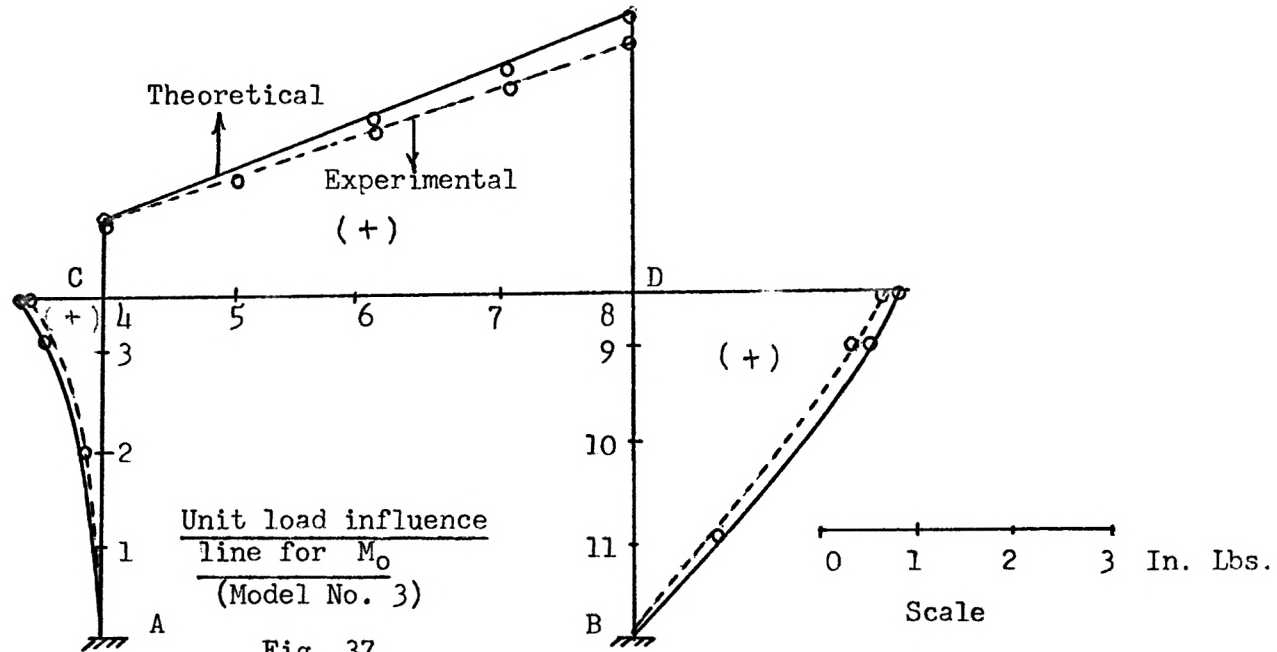


Fig. 37

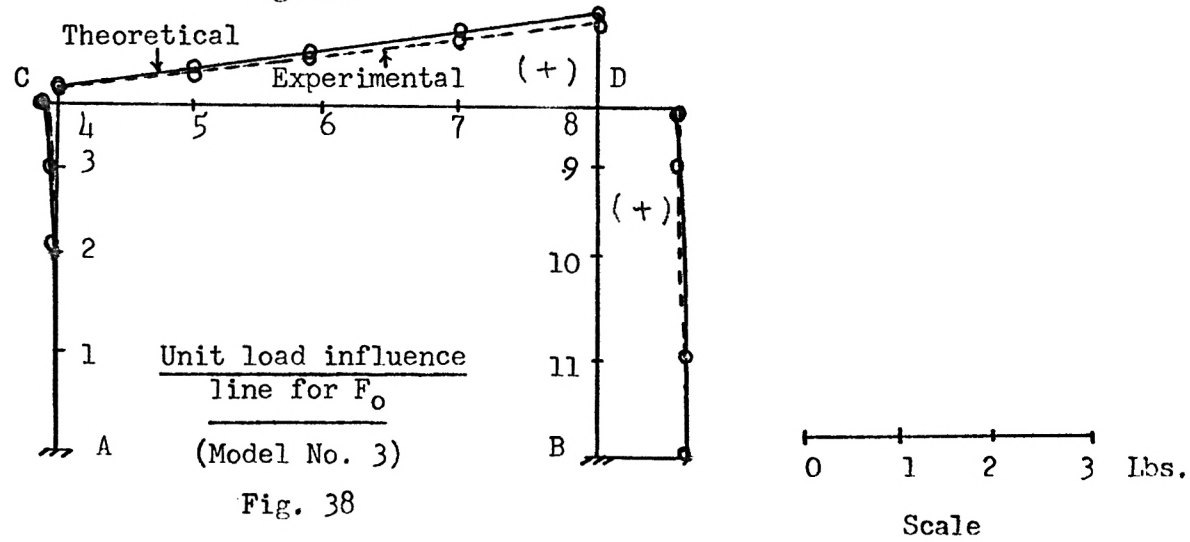
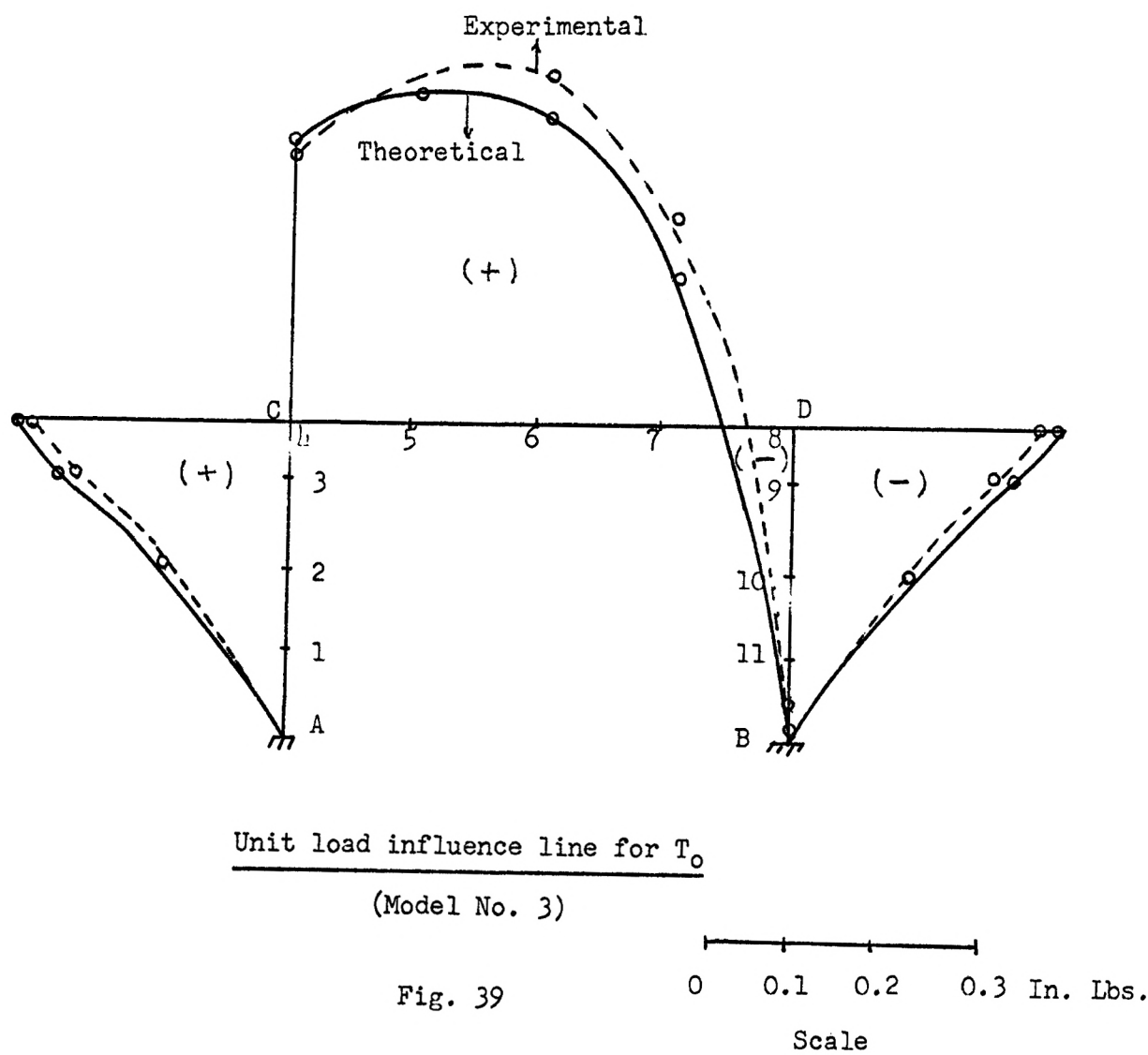


Fig. 38



SUMMARY AND CONCLUSIONS

In this study, the Moire method was used for the analysis of rectangular balcony girder frames, and the results obtained were verified by a strain energy analysis. Black plexiglas was used as the model material and the photographs were taken by a Leica camera with a High Contrast Copy film. A lever was used for the transformation of a vertically suspended load into a horizontally applied load perpendicular to the model surface. Three models of different heights and the same widths were used and the concentrated load was applied at several points along the center-lines of the models to study the effect of a moving load. Photographs of the Moire fringes were obtained by super-imposing on an exposure of the reflection of grid lines at $1/12$ " spacing on the surface of an unloaded model, an exposure of the reflection of the same set of grid lines on the surface of the loaded model. These photographs were analysed by the use of a semigraphical technique of drawing the fringe order versus distance curves from which the bending and torsional moment diagrams were obtained.

The final experimental results were in good agreement with the theoretical results with an average error of 6-7%. It can, therefore, be concluded that the Moire method is a very useful and efficient method for the analysis of complex structures. The great advantage of the Moire method lies not only in its simple apparatus, time saving experimental procedure and comparatively easy calculations, but also in its direction determination of the slopes at different points in the model so that the fringe photographs themselves give a picture of the moment distribution in the model. The influence lines obtained by this method in this study give

a good idea of the effect of lateral loads on rectangular frames of the balcony girder type. They indicate that the most critical load positions to be investigated in the design of these types of structures for bending and torsional moments are the corners C and D, and for shear the fixed ends A and B. The results obtained by the use of Moire method can be considered to be quite adequate for design purposes.

RECOMMENDATIONS FOR FURTHER RESEARCH

The Moire method can be applied to a variety of problems. For example, it can be applied to beams curved in plan with fixed supports or continuous over many supports. It can also be applied to plate problems of any type, stress concentration determination problems or any other stress or strain problems in two dimensions. With modifications in this apparatus, it can also be applied to shell problems, multi-storeyed frame problems and other three-dimensional problems.

The apparatus and the technique need slight improvement because of a few sources of error, already discussed. Precautions should be taken to keep all the portions of the model in complete focus of the camera lens to get complete fringes on all the parts of the model surface. Also, more work should be done before starting the actual experiment to determine the most suitable loads for getting the optimum number of fringes on all the parts of the model. The fringes should be sufficient in number for drawing an accurate fringe order versus distance curve and should not be very closely spaced so that their spacing could be measured very accurately.

LIST OF SYMBOLS

<u>Symbol</u>	<u>Stands for</u>
E -----	Modulus of elasticity in tension and compression
E_t -----	Time dependent modulus of elasticity
EI -----	Bending Stiffness
G -----	Modulus of rigidity
F -----	Shearing Force
F_0 -----	Shearing Force at B
M -----	Bending Moment.
M_0 -----	Bending Moment at B
T -----	Torsional Moment
T_0 -----	Torsional Moment at B
a -----	Distance between the model and the camera
s -----	Distance of the screen from the model which is approximately equal to a
K -----	Transverse deflection at any point on the model
K_x, K_y -----	First partial derivative of K w.r. to x and y, respectively or the slope of the model surface in x and y directions, respectively.
K_{xx}, K_{yy} -----	Second partial derivative of K w.r. to x and y, respectively, or the curvature of the model surface in x and y directions, respectively.
K_{xy}, K_{yx} -----	Second partial derivative of K w.r. to x and y or the warping of the model surface.
K_{xxx}, K_{yyy} -----	Third derivative of K w.r. to x and y, respectively.
ϕ -----	Slope at any point = $\frac{nd}{2a}$

BIBLIOGRAPHY

1. "The Moire method - A new experimental method for the determination of moments in small slab models", by F. K. Lightenberg, Proc. SESA, Vol. XII, No. 2.
2. "New Progress in our knowledge about the moment distribution in flat slabs by means of the Moire method," by C. G. J. Vreendenburgh and H. Van Wijngaarden, Proc. SESA, Vol. XII, No. 2.
3. "Geometry of Moire fringes in strain analysis", by Stanley Morse, August J. Durelli and Cesar A. Sciammarella, Journal of Engg. Mechanics, ASCE, August, 1960.
4. "Structural Model analysis by means of Moire Fringes", by A. J. Durelli and I. M. Daniel, Proc. ASCE (St. 12), December, 1960.
5. "Moire Fringes as a means of analysing strains", by C. A. Sciammarella and A. J. Durelli, ASCE Journal, February, 1961.
6. "Interpretation of Moire Patterns", by A. J. Durelli, C. A. Sciammarella, and V. J. Parks, Journal of Engg. Mechanics ASCE, April, 1963.
7. "The Moire method applied to the three dimensional elastic problems," by C. A. Sciammarella and Fu Pen Chiang, SESA, Vol. XXI, No. 2.
8. "The Moire method and the evaluation of principal moment and stress directions", by Jack G. Bouwkamp, Experimental Mechanics Journal, June 1964.
9. "Isopachic Patterns by Moire method", by Pericles S. Theocaris, Experimental Mechanics Journal, June 1964.
10. "Stress analysis of gridwork models using the Moire method," by Wilhelm K. Kubitza, Ph.D. dissertation submitted to the Washington University, St. Louis, in 1964.
11. "The Moire method of zonal and line gratings", by P. S. Theocaris and H. H. Kuo, Experimental Mechanics Journal, August 1965.
12. "The Moire Grid-Analyser method for strain analysis", by Daniel Post, Experimental Mechanics Journal, November 1965.
13. "A method to increase the accuracy of Moire method", by Fu-Pen Chiang, Journal of Engg. Mechanics, ASCE, Feb. 1965.
14. "Moire Patterns of slope contours in Flexed plates", by Pericles S. Theocaris, April 1966, Experimental Mechanics Journal.

15. "Thermal stresses at high temperatures in stainless steel rings by the Moire method", by C. A. Sciammarella and D. Sturgeon, May 1966.
16. "Basic optical law in the interpretation of Moire patterns applied to the analysis of strains", by B. E. Ross, C. A. Sciammarella and D. Sturgeon, SESA, Vol. XXII, No. 1.
17. "Use of Moire effect to measure plastic strains," by A. Vinckier and R. Dechaene, Trans. ASME, No. 59.
18. "Extension of Moire method to thermal problems", by P. Dantu, Journal of SESA, Vol. XXI, No. 1.
19. "The interference screen method for Isopachic patterns (Moire method)", by G. Mesmer, SESA, Vol. XIII, No. 2.
20. "The determination of moments and deflections in plates by the Moire method", by W. A. Bradley, Ph.D. Dissertation submitted to the University of Michigan in 1956.
21. "The Moire Fringe method of displacement measurement applied to indirect structural model analysis," by R. Shepherd and Wensley, SESA, Vol. XII, No. 1.
22. "The measurement of plane strains by Photoscreen method", by J. D. C. Crisp, SESA, Vol. XV, No. 1, 1957.
23. "The Moire method in thermal fields", by Theocaris, SESA, Vol. XII, No. 2.
24. "The analysis of Engineering structures", by A. J. S. Pippard and J. F. Baker.
25. "Analysis of curved girders", by H. H. Fickel, ASCE, Sept. 1959.
26. "Theory of Structural Analysis and design", by J. Micholas, Ronald Press Co., New York, New York, 1958.
27. "Deflection of circular curve I-beams", by Ross A. Close, ASCE, February 1966.
28. "Elastic Energy Theory", by Van Den Broek.
29. "Materials and Structures", by E. H. Salmon, Vol. I.

APPENDIX

The derivation of the relationship $PQ = 2a\phi \left(1 + \frac{c^2}{a^2}\right)$ is given below:

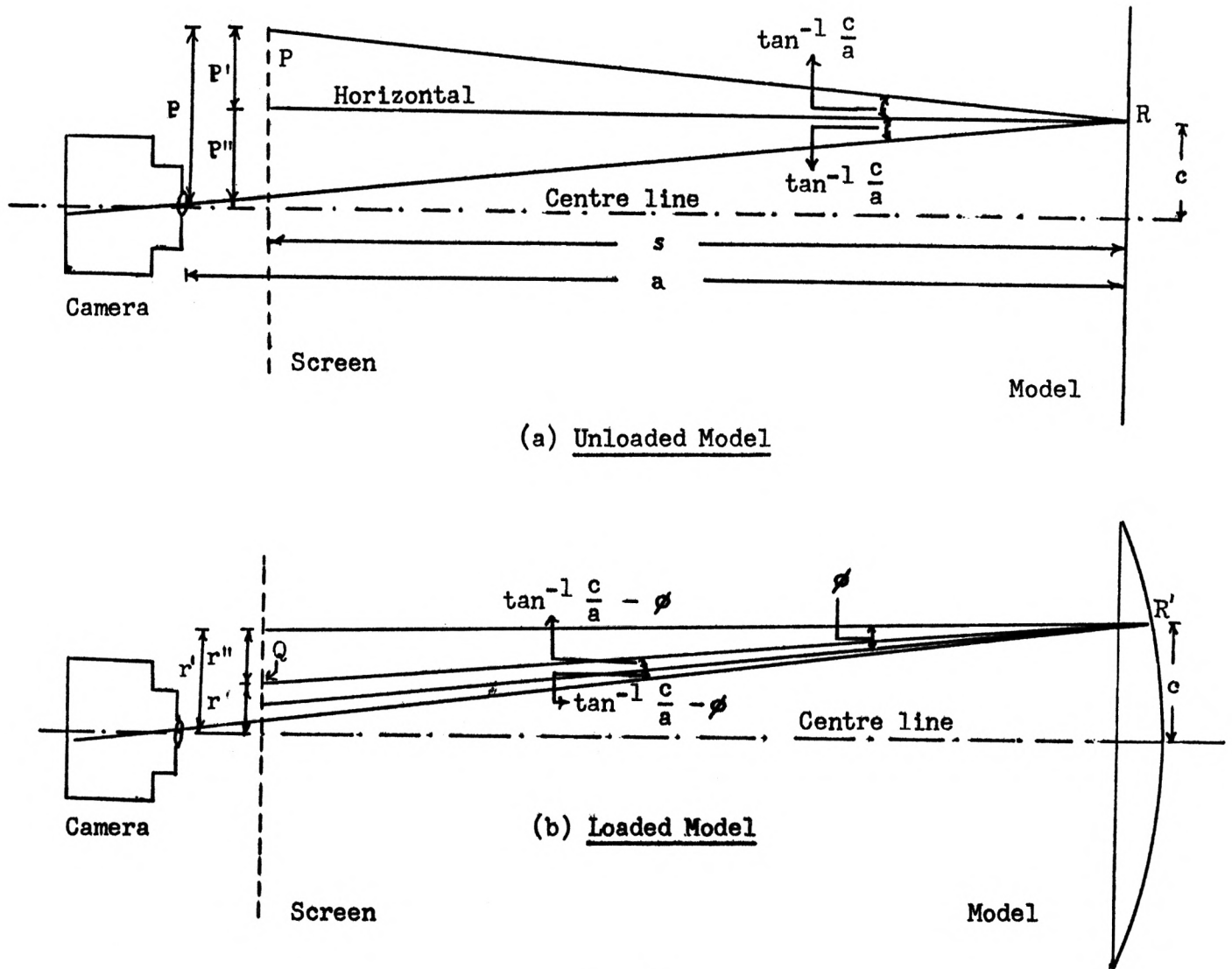


Fig. 40

In order to determine the change in slope ϕ , from the unloaded condition to the loaded condition, we use the known value of the difference $PQ = p - r$,

p being the distance from the axis, of the point on the surface of the grid screen P , reflected to the negative by a given point R on the unloaded model, and r being the distance to the screen point Q , reflected by the same point R' , on the loaded model.

From Fig. (40a), we find,

$$p = p' + p'' = s \cdot \tan(\tan^{-1} c/a) + a \cdot \tan(\tan^{-1} c/a) ,$$

from which $p = (s + a) \frac{c}{a}$ -----(1)

From Fig. (40b), with the deflection of the model RR' neglected as being very small, we obtain

$$\begin{aligned} r = r' + r'' &= a \cdot \tan(\tan^{-1} c/a) - s \cdot \tan[\phi - (\tan^{-1} c/a - \phi)] \\ &= c - s \cdot \tan^{-1} [2\phi - \tan^{-1} c/a] \\ &= c - s \left[\frac{\tan 2\phi - c/a}{1 + (\tan 2\phi) \frac{c}{a}} \right] \end{aligned}$$

But, since ϕ is small, $\tan 2\phi \cong 2\phi$,

$$r = c - s \frac{2\phi - c/a}{1 + 2 \frac{c}{a} \phi} \text{ -----(2)}$$

Combining equations (1) and (2), we obtain

$$p - r = \frac{sc}{a} + c - c + s \left[\frac{2\phi - c/a}{1 + 2 \frac{c}{a} \phi} \right] = \frac{\frac{sc}{a} (1 + \frac{2c}{a} \phi) + s(2\phi - \frac{c}{a})}{1 + 2 \frac{c}{a} \phi}$$

which gives,

$$p - r \cong PQ = \frac{2s\phi + 2s\phi \frac{c^2}{a^2}}{1 + \frac{2c}{a} \phi} \cong 2s\phi \left[1 + \frac{c^2}{a^2} \right] = 2a\phi \left[1 + \frac{c^2}{a^2} \right]$$

since $s \cong a$

USE OF THE MOIRE METHOD IN THE ANALYSIS OF RECTANGULAR
BALCONY GIRDER FRAMES

by

HASAN KAMIL

B.Sc. Engg.(Civil), Aligarh Muslim University(INDIA), 1964

A MASTER'S THESIS

submitted in partial fulfillment of the
requirements for the degree

MASTER OF SCIENCE

Department of Civil Engineering

KANSAS STATE UNIVERSITY

Manhattan, Kansas

1967

The Moire method was used in this study for the analysis of rectangular balcony girder frames. Three models were used with different heights and the same widths and a concentrated load was applied at several points along their centre lines with the aid of a lever arrangement, to study the effect of stationary and moving loads on these types of frames. Photographs of the Moire fringes were obtained by superimposing an exposure of the reflection of a lined screen on the surface of a loaded model over that of the unloaded model. A Leica camera with a high contrast copy film was used for this purpose.

The experimental results were verified with the help of a set of general equations derived by using a Strain Energy method, and gave a very good agreement with the theoretical results.